

# Modified MixNet-Based Classification of Lung Diseases by Using a Noval Dataset



**MCS**

Author

**Ayesha Ahoor**

**Registration Number**

00000364292

Supervisor:

**Assoc. Prof. Dr. Fahim Arif**

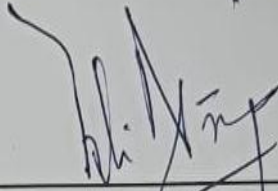
A thesis submitted to the faculty of Computer Software Engineering Department,  
Military College of Signals, National University of Sciences and Technology, Islamabad,  
Pakistan in partial fulfilment of the requirements for the degree of MS in Software

Engineering

November 2023

## THESIS ACCEPTANCE CERTIFICATE

Certified that final copy of MS/MPhil thesis written by Mrs. Ayesha Ahoor, Registration No. 0000364292, of Military College of Signals has been vetted by undersigned, found complete in all respect as per NUST Statutes/Regulations, is free of plagiarism, errors and mistakes and is accepted as partial, fulfillment for award of MS/MPhil degree. It is further certified that necessary amendments as pointed out by GEC members of the student have been also incorporated in the said thesis.

Signature:  \_\_\_\_\_

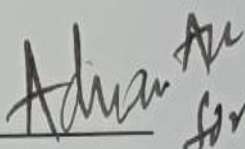
Supervisor: Assoc. Prof Dr. Fahim Arif PhD

Date: \_\_\_\_\_

Signature (HoD):  \_\_\_\_\_

Brig  
Head of Dept of CSE  
Mil College of Sigs (NUST)

Date: 23/11/23

Signature (Dean/Principal):  \_\_\_\_\_

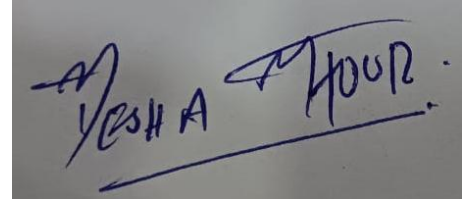
Date: 23/11/23

Brig  
Dean, MCS (NUST)  
(Asif Masood, Phd)

# Declaration

I hereby declare that no portion of work presented in this thesis has been submitted in support of another award or qualification either at this institution or elsewhere.

**Name of Student: Ayesha Ahoor**

A photograph of a handwritten signature in blue ink on a light-colored surface. The signature is written in a cursive style and reads "AYESHA AHOOR". The name is underlined with a single horizontal line.

---

**Signature of Student**

# **Dedication**

“In the name of Allah, the most Beneficent, the most Merciful”

I dedicate this thesis to my family, friends, and teachers who supported me each step of the way.

# Abstract

The lungs are critical components of the respiratory system because they allow for the exchange of oxygen and carbon dioxide within our bodies. However, a variety of conditions can affect the lungs, resulting in serious health consequences. The goal of lung disease treatment is to control their severity, which is usually irreversible. The fundamental goal of this effort is to build a consistent method for automatically establishing the severity of lung illness. This paper describes MixNet-LD, a unique automated approach aimed to identify and categorize the severity of lung illnesses using an upgraded pre-trained MixNet model. One of the first steps in developing the MixNetLD system was to build a preprocessing strategy that uses CLAHE and MSR to decrease noise, highlight irregularities, and eventually improve the classification performance of lung illnesses. Data augmentation strategies were used to rectify the dataset's unbalanced distribution of classes and prevent overfitting. Furthermore, dense blocks were used to improve classification outcomes across the four severity categories of lung disorders. In practice, the MixNet-LD model achieves cutting-edge performance while keeping the model size and complexity manageable. The proposed approach was tested using a variety of datasets gathered from credible internet sources, as well as a novel private dataset known as Pak-Lungs. A pretrained model was used on the dataset to obtain important characteristics from lung disease images. The pictures were then categorized into categories such as Normal, COVID-19, Pneumonia, Tuberculosis, and Lung Cancer using a linear layer of the SVM classifier with a linear activation function. The MixNetLD system was tested in four distinct tests and achieved a remarkable accuracy of 98.5% on the difficult lung disease dataset. The acquired findings and comparisons clearly demonstrate the MixNet-LD system's improved performance and learning capabilities. These findings show that the proposed approach may effectively increase the accuracy of classification models in medicinal image investigation. This research helps to further the development of new strategies for effective medical image processing in clinical settings.

# Acknowledgements

All praises to Allah for the strengths and His blessing in completing this thesis.

I would like to convey my gratitude to my supervisor, Assoc Prof Dr. Fahim Arif, PhD, for his supervision and constant support. His invaluable help of constructive comments and suggestions throughout the experimental and thesis works are major contributions to the success of this research. Also, I would thank my committee members; Assoc Prof Dr. Ehtisham ul Islam, and Asst Prof Dr. Nauman Ali Khan for their support and knowledge regarding this topic.

Last, but not the least, I am highly thankful to my family, friends and teachers. They have always stood by my dreams and aspirations and have been a great source of inspiration for me. I would like to thank them for all their care, love and support through my times of stress and excitement.

## Table of Contents

Declaration .....	ii
Dedication .....	iii
Abstract .....	iv
Acknowledgements .....	v
Introduction .....	1
1.1. Introduction .....	1
1.2. Research Motivation.....	2
1.3. Research Contribution.....	3
1.4. Thesis Outline.....	4
1.5. Summary .....	5
Literature Review.....	6
2.1. Overview .....	6
2.2. Estimation of DL Models.....	7
2.3. CT Scan for COVID-19 Detection.....	7
2.4. D-Rest-net Model Used for COVID-19.....	8
2.5. CNN Model Trained by Using CT & X-ray Images .....	10
2.6. Summary .....	12
Inception V3, VGG16 and VGG19 Architecture .....	14
3.1. Overview .....	14
3.2. Inception V3.....	14
3.3. VGG16 Model.....	20
3.4. VGG19 Model.....	24
3.5. Summary .....	27
Proposed Methodology & Framework.....	28
4.1. Overview of Proposed Methodologies.....	28
4.2. Proposed Approach .....	29
4.3. Dataset Acquisition and Pre-processing.....	30
4.4. Data Augmentation .....	32
4.5. MixNet-LD Architecture.....	35

4.6. Recognition of Lungs Disease .....	40
4.7. LSVM.....	41
4.8. Summary .....	43
Results and Experiments.....	44
5.1. Overview .....	44
5.2. Experiment 1: Performance Comparison between MixNet LD, VGG16, VGG19, Inception V3, ResNet.....	45
5.3. Experiment 2: Proposed Model Training and Validation Accuracy & Loss on Public Dataset.....	46
5.4. Experiment 3: Proposed Model Training and Validation Accuracy & Loss on Public Dataset.....	47
5.5. Experiment 4: Performance Comparison between Chest CT-Scan Images Dataset & Pak Lungs (Cancer).....	49
5.6. Summary .....	51
Analysis and Discussion .....	52
6.1. Overview .....	52
6.2. State of the Art Comparison.....	52
6.3. Discussion .....	54
6.4. Summary .....	56
Conclusion .....	57
7.1. Conclusion .....	57
References.....	59



## List of Figures

Figure 1.1: Illustration of Lungs Disease .....	4
Figure 3.1: Take the Conception V1 Module's Basic Module as an Illustration .....	16
Figure 3.2: Convolutional Layers in Order .....	16
Figure 3.3: Two 33 Convolutions Minimize. ....	17
Figure 3.4: Asymmetric Convolutions .....	18
Figure 3.5: Structure of Asymmetric Convolutions .....	19
Figure 3.6: Efficient Grid Size Reduction .....	20
Figure 3.7: Inception V3 Architecture .....	20
Figure 3.8: Inception V3 Model Layers .....	21
Figure 3.9: VGG16 Model Layers .....	22
Figure 3.10: VGG 16 Architecture .....	24
Figure 3.11: VGG 19 Architecture .....	28
Figure 4.1: The MixNet-LD system's well-organized flow diagram for identifying lung illness ..	31
Figure 4.2: This image represents pre-processing results after Gran Cam technique. ....	33
Figure 4.3: Schematic diagram of MixNet-LD .....	40
Figure 4.4: Dense Blocks .....	42
Figure 5.1: Comparison between different DL model and MixNet-LD .....	47
Figure 5.2: Represents the proposed model's training validation accuracy and loss. ....	48
Figure 5.3: Confusion matrix of Lungs Diseases Dataset (4 Types) .....	48
Figure 5.4: Represents the proposed model's training and validation accuracy and loss using Pak Lungs. ....	49
Figure 5.5: Confusion matrix of Pak-Lungs Dataset .....	50
Figure 5.6: Confusion matrix of Pak-Lungs (Cancer) .....	51
Figure 5.7: Training validation accuracy and loss on Pak-Lungs (Cancer) .....	51

## List of Tables

Table 2.1. An Examination & Comparison of the Current Studies .....	12
Table 3.1. 16 Layer of VGG16 .....	23
Table 3.2. VGG 19 Layers .....	26
Table 4.1. Image dataset of the lungs diseases for the MixNet-LD system .....	32
Table 4.2. Image dataset of the lungs cancer for the MixNet-LD system .....	32
Table 4.3. Image dataset of the lungs diseases for the MixNet-LD system .....	34
Table 4.4. Image dataset of the lungs cancer for the MixNet-LD system .....	34
Table 4.5. Algorithm 1: Auto Augmentation .....	35
Table 4.6. Algorithm 2: Working of the MixNet-DL model for feature map extraction .....	38
Table 4.7. Symbolization Table .....	42
Table 4.8. Proposed LSVM classifier .....	44
Table 5.1. Performance comparison between MixNet-LD, VGG16, VGG19, InceptionV3, ResNet, Xception and MobileNet .....	46
Table 5.2. Performance assessment between Lungs Diseases Dataset (4 Types) and Pak-Lungs	49
Table 5.3. Performance comparison between Chest CT-Scan Images Dataset and Pak-Lungs (Cancer) .....	51
Table 6.1. performance comparison between Incept-HR, Trivijoyo-2017 and CAD-HR .....	54

## Introduction

### 1.1. Introduction

DL algorithms (DLAs) have transformed the area of medicinal image investigation, promising advances in lung disease identification and classification. Based on significant research articles in the field, this introduction provides a general idea of the application of DL models in identifying and categorizing various lung illnesses such as pneumonia, tuberculosis (TB), COVID-19, and lung cancer. Wang et al. [1] released the ChestX-ray8 dataset, which has been critical in the development of DL models for chest X-ray processing. This dataset, in conjunction with standards for weakly-controlled organization and localization of common thoracic disorders, has laid the groundwork for diagnosing pneumonia and other lung anomalies. Furthermore, CNNs have determined remarkable functioning in lung disease diagnosis. Shen et al. [2] presented multi-scale dense networks that use deep CNN architectures for efficient picture categorization. Through the extraction of hierarchical characteristics, this technique has proved its usefulness in accurately identifying lung illnesses. The COVID-19 epidemic has established an important requirement for precise and speedy diagnosis. Li et al. [3] created an AI system that can identify COVID-19 from communal-developed pneumonia on chest CT images. By utilizing DL techniques, this system assists in the detection and distinction of COVID-19 patients, helping to enhanced disease managing and controller. TB, another major lungs illness, has also been the subject of DL research. Lakhani and Sundaram [4] presented a DL model for automated pulmonary TB classification on chest radiography. Their method identified TB-related anomalies with high accuracy, allowing for quick screening and diagnosis. Their model showed encouraging results in recognizing and distinguishing patterns associated with distinct interstitial lung illnesses, allowing for more precise diagnosis and treatment planning. Furthermore, the use of DL in COVID-19 diagnosis has received a lot of interest. Apostolopoulos and Mpesiana [5] used transfer learning and CNNs to detect COVID-19 in X-ray pictures. Their technique demonstrated the power of DL in supporting radiologists and health care workforces in detection COVID-19 patients quickly. Anthimopoulos

et al. [6] developed a deep CNN for lung pattern categorization, with a focus on interstitial lung disorders. Furthermore, Jin et al. [7] created and tested an AI system for COVID-19 analysis. DL techniques were used in this approach to help in the accurate recognition of COVID-19 patients from imaging data. Rajpurkar et al. [8] presented the CheXNeXt technique to increase the scalability and efficiency of DL models, which displayed equivalent performance to practicing radiologists in identifying a wide range of diseases in chest radiographs. Their research demonstrated the use of DL models in helping radiologists and improving the accuracy of lung disease diagnosis. Lopes et al. [9] concentrated on tuberculosis screening, creating a DL system that detects TB-related anomalies on chest radiographs. Their research yielded encouraging findings in identifying those at high risk of TB, allowing for prompt intervention and treatment. DL models have been intensively explored for lung cancer diagnosis, in addition to infectious disorders. Kermany et al. [10] created an image based DL system that can detect medical diagnoses and curable illnesses such as lung cancer.

This model demonstrated the power of DL in identifying lung cancer and other illnesses.

This extensive study gives important insights into the creation of DL models for the identification of pneumonia, TB, COVID-19, and lung cancer. They show how DL can reliably detect and categories lung disorders, resulting in improved patient consequences and more effective healthcare administration. We want to use the advances provided in these studies, as well as other relevant research, to construct a complete DL model for lungs illness recognition and classification in this work. Our study aims to improve the accuracy, efficiency, and consistency of lung illness detection by analyzing varied datasets and applying cutting-edge approaches, ultimately leading to better patient care and treatment.

## **1.2. Research Motivation**

Despite the development of various approaches for diagnosing lung disorders from photographs, such as Normal, COVID-19, Pneumonia, Tuberculosis, and Lung Cancer, substantial hurdles remain.

- Despite the use of advanced technologies for image processing both during and after acquisition., defining lung features from images associated with Normal, COVID-19,

Pneumonia, Tuberculosis, and Lung Cancer remains difficult due to the struggle in emplacement and extracting lesion features associated with lung diseases.

- Professional medical annotations are restricted in publicly available datasets encompassing a varied array of Normal, COVID-19, Pneumonia, Tuberculosis, and Lung Cancer-related damage variables. As a result, computerized systems have difficulty precisely diagnosing the symptoms of certain disorders.

As a finding, the foremost aim of this research is dual. For starters, it intends to develop a complete dataset for the classification of Normal, COVID-19, Pneumonia, Tuberculosis, and Lung Cancer (abbreviated PAK-LUNGS). Second, the study aims to create a comprehensive multilayered DL model capable of autonomously interpreting pictures relevant to lung disorders, especially in the setting of lung-associated ailments. To do this, a multilayered MixNet system is used to build a MixNet-LD system with dense blocks. By fully training this MixNet-LD system, it becomes skilled at reliably recognizing lungs illnesses on diverse pictures connected to lungs associated maladies, including anatomic component recognition. A skilled pulmonologist discovered these illnesses and anatomical traits. This work is significant because it proposes a revolutionary categorization system for lung disorders, with potential real-world implications in medical diagnosis and therapy.

### **1.3. Research Contribution**

We proposed a new DL model inside this framework to handle the difficulty of identifying diverse lung illnesses. In addition, we give PAK-LUNGS, a freshly curated dataset acquired from hospitals in Pakistan. The following are the noteworthy contributions of the MixNet-LD system:

- The researchers created an enormous dataset called "Pak-LUNGS" for this study by gathering 6,000 photos from Pakistani hospitals and other internet resources. This large dataset was critical in allowing the trained model to attain exceptionally high classification accuracy.
- The study used dense blocks and trained MixNet CNN to build the MixNet-LD system, resulting in a multi-layered architecture capable of efficiently handling the classification issue.

- The MixNet-LD model's system design includes four extra layers to identify lung-related disorders. The CNN model is used to extract lung-related lesion characteristics, which are subsequently enlarged upon using the dense block approach.
- The method proposed in this work for categorizing lung disorders is based on the deep features and phases of color space, which constitute the foundation of the approach. According to the author, this is the first effort to develop a computerized technique that outperforms existing techniques in detecting Normal, COVID-19, Pneumonia, Tuberculosis, and lung cancer disorders.
- Our systems outperformed the proposed approaches in the current literature with a much higher accuracy of 95%.

## 1.4. Thesis Outline

This thesis is divided into seven chapters:

- **Chapter 1:** This chapter includes the basic introduction, establish the research motivation and research contribution.
- **Chapter 2:** This chapter describes the literature survey of articles related to this research.
- **Chapter 3:** This chapter describes the different deep learning models.
- **Chapter 4:** This chapter describes the proposed architecture.
- **Chapter 5:** This chapter describes the experiments results.
- **Chapter 6:** This chapter compares our work with state-of-the-art research.
- **Chapter 7:** This chapter presents the discussion on the overall research.
- **Chapter 8:** This chapter concludes the report and highlights the direction for future work.



*Figure 1.1: Illustration of Lungs Disease*

## **1.5. Summary**

The revolutionary effect of Deep Learning Algorithms (DLAs) on medical image analysis is covered in this chapter, with special attention to how they affect the diagnosis and categorization of lung diseases. It emphasizes important studies and advancements in the area, such as the use of DL models to diagnose COVID-19, lung cancer, pneumonia, and tuberculosis (TB). The chapter provides an introduction to the datasets and DL approaches that have advanced the detection of lung diseases.

The section on study motivation highlights the persistent difficulties in precisely identifying lung characteristics from medical pictures and the scarcity of annotated datasets for automated system training. In response to these difficulties, the chapter describes the research's two main goals: building a multilayered deep learning model (MixNet-LD) that can analyze lung-related pictures on its own and building a comprehensive dataset (PAK-LUNGS) for the purpose of identifying different lung disorders. The PAK-LUNGS dataset from Pakistani hospitals, the development of the MixNet-LD model with improved classification capabilities, to classify lung illnesses are just a few of the notable accomplishments highlighted in the research contribution section. According to the author, their method outperforms current methods with a 95% accuracy rate.

# Literature Review

## 2.1. Overview

An overview of the use of deep learning (DL) models for lung disease classification and diagnosis, including pneumonia, TB, COVID-19, and lung cancer, is given in this chapter. These illnesses have high rates of morbidity and death worldwide, making them serious public health problems. Proper and timely diagnosis is essential for successful therapy and better patient outcomes.

In medical image analysis, deep learning models have shown potential, especially when it comes to automating the diagnosis and categorization of lung diseases. X-rays and chest computed tomography (CT) scans are frequently utilized diagnostic procedures, particularly for COVID-19. Transfer learning techniques, using models like as VGG-16, ResNet-50, and InceptionV3, have shown promising outcomes in the analysis of clinical pictures associated with respiratory disorders, such as pneumonia and COVID-19.

DL models have been shown in many studies to be useful in the identification of COVID-19 patients based on chest X-ray (CXR) and CT scan images. These models exceed conventional techniques with their excellent accuracy and precision. Furthermore, DL models have been used to distinguish between COVID-19 instances that are severe and those that are not.

With an emphasis on CT scans, the chapter also covers the use of DL models in the diagnosis and categorization of lung cancer. Improving survival rates from lung cancer requires early identification, and DL models have shown potential in this area. To diagnose lung cancer from medical pictures, many DL architectures have been utilized, such as DenseNet and MLP classifiers.

Overall, this chapter demonstrates the great potential of deep learning models for lung disease classification and diagnosis, providing hope for more precise and effective medical image analysis in the area of respiratory health.



## **2.2. Estimation of DL Models**

Lung illnesses, such as pneumonia, TB, COVID-19, and lung cancer, are major public health issues globally, resulting in considerable morbidity and death rates [11]. Early and precise diagnosis and categorization of these disorders is critical for prompt treatment and improved patient outcomes. DL models have established encouraging outcome in medical image analysis in recent years, enabling automated identification and categorization of lung disorders [12]. In many countries, chest computed tomography (CT) and X-ray scans are employed as a reasonable approach for identifying COVID-19. Identifying COVID-19, on the other hand, is a complicated job that needs clinical imaging of patients [13-14]. Lung cancer has a foremost influence on human impermanence, making early detection critical for increasing survival rates (15-18). The combination of machine learning and image processing has shown significant ability in improving lung cancer diagnosis.

This partition discusses a complete estimation of DL models for tuberculosis, COVID-19, lung cancer, and pneumonia. The application of transfer learning approaches to clinical pictures of lung illnesses and COVID-19, such as VGG-16, ResNet-50, and InceptionV3, has given encouraging results. Pneumonia has been identified as a key symptom of COVID-19, and transfer learning has indicated that both pneumonia and COVID-19 are caused by the same virus. A model trained to perceive disease-causing pneumonia was shown in a research to be capable of detecting COVID19. Haralick characteristics were used to help in feature extraction, with statistical analysis focusing on a specific region of COVID-19 diagnosis. Transfer learning frequently produces statistically significant results when compared to standard classifications [13].

## **2.3. CT Scan for COVID-19 Detection**

Several research has used CT scans to design and test completely automated COVID-19 detection frameworks. COVID-19 neural network techniques were utilized to obtain graphical information from volumetric chest CT images. The findings show that this strategy outperforms previous approaches. In related work, pre-trained model-based CNNs such as InceptionResNetV2, ResNet152, ResNet50, InceptionV3, and ResNet101 were used to detect COVID-19 pneumonia based on CXR pictures. ResNet50 produced the best accurate categorization results among these

models [19]. CT scans from 101 pneumonia patients, 88 COVID-19 patients, and 86 healthy cases from two sites in China were used for the comparison and modelling.

Furthermore, COVID-19 patients were identified using the Details Relation Extraction Neural Network, a DL-based CT diagnostic technique. With a recall of 0.93, an AUC of 0.99, and an accuracy of 0.96, the model made valid distinctions. Permitting to the findings, DL based on CT scans could be useful in diagnosing COVID-19 patients and automatically recognizing potentially problematic alterations. Another research used a transformed MobileNet and a ResNet architecture to classify COVID-19 CXR pictures. To avoid the gradient vanishing problem, this methodology dynamically merged characteristics from different CNN layers, and the suggested approaches surpassed current techniques with accuracies of 99.3% on the CT image dataset and 99.6% on the CXR images [20].

## **2.4. D-Resnet Model Used for COVID-19**

Several research [21] have built models to differentiate relating dangerous and relentless COVID19 patients using DL features and radionics based on D-Resnet. These trials included 217 people from three Chinese hospitals, with 82 classed as having great strictness and 135 as having critical sickness. The patients were separated into two groups: training (174 patients) and testing (43 patients). The researchers built a 3-dimensional DL network using clipped segments and multivariable logistic regression to incorporate key radionics features and DL scores. They used stratified analysis, cross-validation, decision curve analysis, and survival analysis to test the robustness of their approaches. The AUC for identifying critical patients in the test and training groups was 0.909 [22].

Additional research used InceptionV3, NASNet, Xception, DenseNet, MobileNet, VGGNet, InceptionResNetV2, and ResNet to classify COVID-19 cases on a mixed dataset of CXR and CT images. DenseNet121 performed the best, with an accuracy of 99% [21]. In one study, an image segmentation approach was used to classify chest CT scans as pneumonia, COVID-19, or normal diseases. Four CNN base learners, a transformed stack ensemble model, and Naive Bayes as the meta-learner were used in the technique. On typical datasets based on CT scans, this strategy surpassed current approaches with an accuracy of 0.9867 and a Kappa of 0.98. The proposed method eliminates the requirement for manual labelling while reliably detecting COVID-19

infections and excluding out non-COVID-19 cases [23]. Positive qualitative and quantitative results point to wider application in large-scale clinical studies. Using decision trees, Inception V2, and VGG-19 models, convolution neural networks were proven to be successful at categorizing 360 X-ray and CT scan pictures into a binary class pneumonia-based translation. When compared to decision tree and Inception V2 models, the fine-tuned version of VGG-19 had the greatest gain in training and validation precision [24]. GSA-DenseNet121-COVID-19, a novel hybrid CNN architecture based on DenseNet121 and the gravitational search optimization approach (GSA), was developed. Other DenseNet121 models, which could only diagnose 94% of the test set, were surpassed by this design. The GSA-DenseNet121-COVID-19 approach outperformed an Inception-v3 CNN architecture and instructions assessment for obtaining hyper parameter evaluations, categorizing 95% of the test set samples [25].

Kernel principal component analysis was used to decrease pre-trained Efficient-Net models. A feature fusion approach was worked to merge the extracted features. Stacked ensemble met classifiers were used to divide the model into two phases. Predictions were created in the first stage using a support vector machine (SVM) and a random forest, which were then combined and input into the second stage. During the second step, a logistic regression classifier classified the X-ray and CT data into two groups: COVID and NON-COVID. When compared to previous CNN-based pre-trained models, the new model outperformed them, making it a viable tool for doctors in point of-care diagnostics [26].

In a similar study, researchers classified COVID-19-infected individuals using ResNet32 and a deep transfer learning approach. The experimental results demonstrated that their COVID-19 classifier outperformed earlier supervised learning models, producing improved results [27]. Another cutting-edge attention-based DL model was created, this time with VGG-16 and a finetuned classification procedure tailored exclusively for COVID-19 detection. When compared to current models, the suggested technique displayed consistent and promising performance. In the instance of InstaCovNet-19, a unique integrated stacking deep convolutional network was used, with pre-trained models such as ResNet101 and XceptionV3 being used. The model has an accuracy of 0.99 for three classes (Normal, Pneumonia, and COVID-19) and a precision of 0.9953 for two classes (COVID and non-COVID). The proposed model achieved 98% accuracy in ternary classification and 100% precision and 98% recall in binary classification [28].

## 2.5. CNN Model Trained by Using CT & X-ray Images

For both binary and multiclass classification, a CNN was utilized. The model was trained using 3,877 CT and X-ray images, including 1,917 from COVID-19 patients. The binary classifier has 99.64% accuracy, a 99.58% recall, a 99.56% precision, a 99.59% F1 score, and a 100% ROC. The recommended approach achieved 98.28% accuracy, 98.25% recall, 98.22% precision, 98.23% F1score, and 99.87% ROC using 6,077 pictures, comprising 1,917 COVID-19 patients, 1,960 healthy persons, and 2,200 pneumonia patients [29].

Early identification of lung cancer increases survival odds from 14% to 49%. While CT techniques are more reliable than X-rays, a definitive diagnosis frequently requires the use of numerous imaging modalities. To address this, an artificial DNN for detecting lung cancer in CT scans has been created. For identifying lung pictures as normal or cancerous, studies have proposed an adaptive boosting approach using a DenseNet. Using a training dataset of 201 lung images, the suggested technique obtained 90% accuracy in testing, with 85% for training and 15% for testing and classification [18]. An MLP classifier beat other classifiers with an accuracy of 88.55% in another investigation [17].

Using CT images of benign and malignant lung nodules from the LIDC database, CNN, DNN, and sparse auto-encoder deep neural networks were used to identify lung cancer calcification, reaching an accuracy of 84.15%, sensitivity of 83.96%, and specificity of 84.32% [16]. CNN was shown to be the most accurate of the three networks tested.

One study used an artificial neural network, ensemble classifier, SVM, and KNN for categorization of COVID-19 and pneumonia, with a DL architecture of RNN with LSTM suggested to identify lung diseases, demonstrating robustness and efficacy [31]. Another study classified data using an ensemble of InceptionResNet\_V2, ResNet50, and MobileNet\_V2, with ResNet50, MobileNet\_V2, and InceptionResNet\_V2 models yielding the best F1 score of 94.84% [32].

Through transfer learning approaches, CNN with pre-trained weights was used to categorize COVID-19, pneumonia, and healthy persons, accurately identifying those with active SARSCoV2 and pneumonia, a noteworthy discovery in that work [30].

Using Retina Net and Mask R-CNN as an ensemble, machine learning was used to detect and localize pneumonia in CXR, attaining a recall of 0.793 for a large dataset [33]. Transfer learning

was used to acquire pictures from CXR and CT scans in the context of diverse lung illnesses. A unique architecture was trained to detect virus-related pneumonia in order to detect COVID-19.

The findings of transfer learning differed markedly from those of standard categories [34]. One research created a CNN model from scratch to extract and categorize information from chest X-ray pictures of people sick with pneumonia, with the goal of addressing issues associated with medical image analysis. Due to the scarcity of pneumonia datasets, different data augmentation procedures were used to improve the proposed model's training and validation classification accuracy, resulting in a substantial precision of 0.94814 during the validation phase [35]. A transfer learning system was used to distinguish between CXR images labelled as showing pneumonia and those categorized as normal, using weights pre-trained on ImageNet using the Xception Network. When compared to current techniques, the model produced competitive results, with accuracy, recall, F1, and ROC values of 0.84, 0.91, 0.99, and 0.97, respectively [38]. In a different investigation, experts looked at 180 X-ray images of COVID-19-infected individuals and attempted to identify the virus using effective programmers like the ResNet50V2 and Xception networks. For all classes and COVID-19 examples, the suggested model was 99.50 percent accurate. [36].

Furthermore, researchers constructed a DCNN model to identify TB using a CXR dataset from the National Library of Medicine Shenzhen No.3 Hospital. The datasets that were analyzed to a separate population's non-TB-specific chest X-ray dataset. For the two datasets, the DCNN provided AUC values of 0.9845 and 0.8502, respectively, whereas the supervised DCNN model in the CXR dataset had a lower AUC of 0.7054. In the CXR dataset, the final DCNN model successfully identified 36.51% of the abnormal radiographs associated with TB [39]. Another research used ResNet and depth-ResNet to predict severity ratings and analyze the risk of TB. For TB detection, depth-ResNet obtained 92.70% accuracy, whereas ResNet-50 achieved 67.15% accuracy. The study used severity probabilities to translate scores into probabilities of 0.9, 0.7, 0.50, 0.30, and 0.2 for high severity (scores 1 to 3) and low severity (scores 4 and 5). Both techniques have average accuracies of 75.88% and 85.29%, respectively [40].

Other research presented an ensemble approach based on three well-known designs: AlexNet, GoogleNet, and ResNet. For training and testing, a new classifier for tuberculosis classification was created from scratch utilizing a pooled dataset of publicly available standard datasets. The suggested strategy outperformed most current algorithms with an accuracy of 88% and an AUC of

0.93 [41]. The extraction of features in a hierarchy for the identification of abnormalities approach divides attributes into healthy and unhealthy groups using two levels of hierarchy. Level one comprises the extraction of handcrafted geometrical features, while level two covers the extraction of typical statistical features and textural features from segmented lung fields. The method was evaluated on 800 CXR pictures from two public datasets, yielding AUC values of 0.99 and 0.01 for Shenzhen and 0.95 and 0.06 for Montgomery, respectively, demonstrating promising performance when compared to previous methodologies [42]. Friedman's post hoc multiple comparison methods were also used to statistically validate the proposed strategy.

Machine learning-based classification-based detection for COVID-19 was introduced in [43,44].

Table 2.1. summarizes the research on the identification and categorization of chest illnesses.

*Table 2.1. An Examination & Comparison of the Current Studies*

Ref No	Methodologies	Disease	Dataset
[13]-[28]	VGG-16, ResNet-50, InceptionV3, VGG19 + ResNet-50, DRENet, Modified ResNet, ResNet50, DenseNet121, VGG16, D-Resnet-10 network, VGG + CNN, VGG-16, InceptionV2, DT, GSA-DenseNet121, DL Meta classifier, ResNet32 + DTL, VGG-16, InstaCovNet-19.	COVID-19	CXR+CT
[15]-[18]	FPSO-CNN, Multilayer Perceptron (MLP), CNN, MGSA.	Lungs Cancer	CT
[31]-[37]	RNN-LSTM, ResNet50 + MobileNetV2 + InceptionResNetV2, CNN with pre-trained weights on ImageNet, RetinaNet and Mask R- CNN, Transfer learning, CNN, Xception Network pretrained weights on ImageNet, Xception + ResNet50V2.	Pneumonia	CXR+CT
[39]-[42]	DCNN, Depth- ResNet Ensemble (AlexNet, GoogleNet, and ResNet), SVM + FOSF + GLCM.	Tuberculosis	CXR, CT

## **2.6. Summary**

The substantial effects of lung diseases on worldwide public health, such as pneumonia, TB, COVID-19, and lung cancer, are covered in this chapter. For these illnesses, early and accurate diagnosis is critical, and deep learning (DL) models have shown potential for automating the recognition and classification of various lung ailments. The chapter examines the diagnosis of COVID-19 and other lung disorders from medical pictures using deep learning models and transfer learning techniques including VGG-16, ResNet-50, and InceptionV3. It also emphasizes the promise of DL in the identification of lung cancer and the efficacy of DL-based techniques in identifying important COVID-19 patients.

The research covered in this chapter uses a variety of DL models and approaches on a range of medical picture types, such as X-ray, CT, and chest computed tomography scans. These techniques have shown encouraging outcomes in the identification and classification of COVID-19 patients, pneumonia, and lung cancer. Numerous studies have shown the potential of deep learning (DL) to improve patient outcomes by enabling early diagnosis, with high accuracy rates in diagnosing certain disorders.

With an emphasis on COVID-19, pneumonia, tuberculosis, and lung cancer in particular, this chapter offers an overview of the methods being utilized to diagnose and classify lung disorders using DL models and transfer learning methodologies. Numerous research findings support the usefulness of these techniques in raising diagnostic precision and maybe saving lives.

# Inception V3, VGG16 and VGG19 Architecture

### 3.1. Overview

In the framework of deep learning and convolutional neural networks (CNNs), this chapter discusses the VGG16 and VGG19 models and gives an overview of the Inception V3 model. Presented in 2015, Inception V3 is a 42-layer deep neural network that offers more accuracy than its predecessors.

With 16 convolutional layers and a unified architecture, the VGG16 is a variation of the VGG model. According to the chapter, VGG19 needs 19.6 billion floating-point operations (FLOPS) in order to do inference.

The chapter provides a short overview of CNNs—specifically, VGG19—used in picture identification as well as ImageNet, a large image database.

### 3.2. Inception V3

The Inception v3 model, which was introduced in 2015, has 42 layers overall and a reduced mistake rate than its forerunners. Let's examine the many improvements that the Inception V3 model has received. The Inception V3 model has changed significantly, including:

- Factorization into Smaller Convolutions
- Spatial Factorization into Asymmetric Convolutions
- Utility of Auxiliary Classifiers
- Efficient Grid Size Reduction

Let's examine the implementation of each of these improvements and how they benefited the model.



### 3.2.1. Factorization into Smaller Convolution

The extensive dimension reduction was one of the Inception V1 model's key advantages. The model's bigger Convolutions were factorized into smaller Convolutions to make it even better.

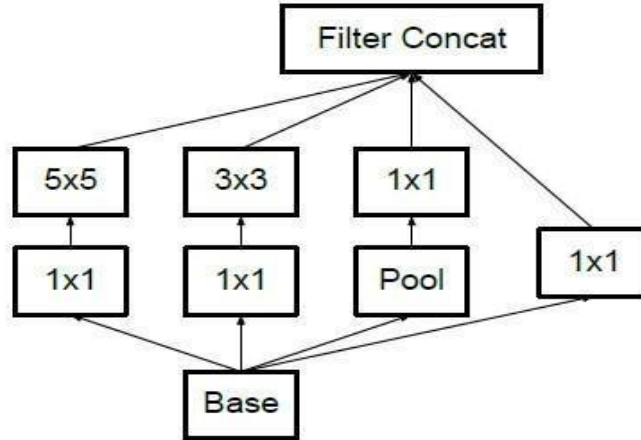


Figure 3.1: Take the Inception V1 Module's Basic Module as an Illustration

It contains a 55 convolutional layer, which as was previously said was computationally costly. The 55 convolutional layer was therefore replaced with two 33 convolutional layers in order to lower the computational cost, as seen below.

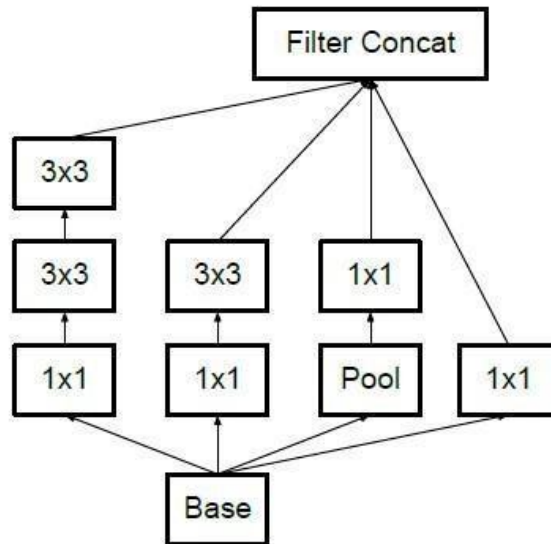


Figure 2.2: Convolutional Layers in Order

See how the use of two 3x3 convolutions minimizes the amount of parameters to have a better understanding of it in figure 3.3.

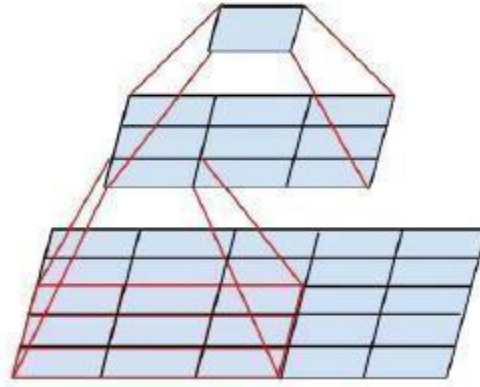


Figure 3.3: Two 3x3 Convolutions Minimize.

The computing expenses also decrease as a result of the fewer parameters. A relative gain of 28% was obtained as a result of factorizing bigger convolutions into smaller convolutions.

### 3.2.2. Spatial Factorization into Asymmetric Convolutions

Despite the fact that bigger convolutions are split into smaller convolutions. You might be curious what would happen if we were to factorize any more, perhaps to a 2x2 convolution. But asymmetric convolutions were a superior option to improve the model's efficiency.

#### 3.2.2.1. Asymmetric convolutions are of the form $n \times 1$

They therefore substituted a 1x3 convolution followed by a 3x1 convolution for the 3x3 convolutions. This is equivalent to sliding a two-layer network with a 3x3 convolution's receptive field.

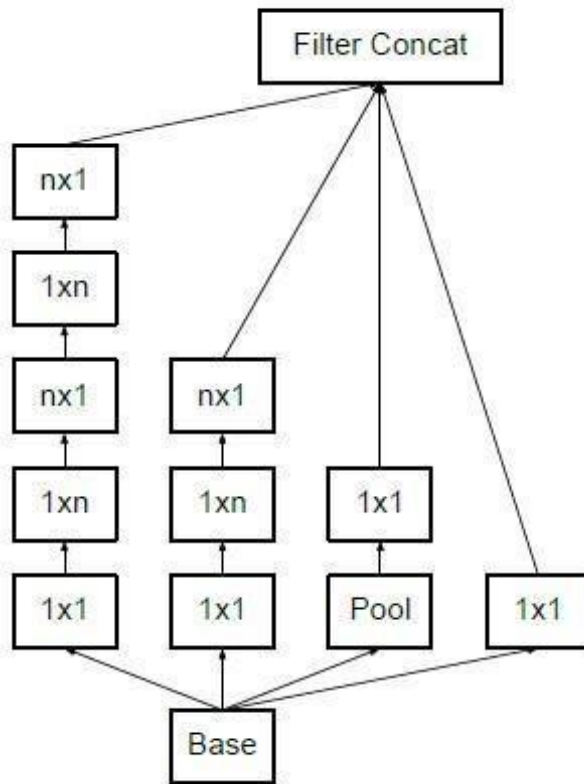


Figure 3.4: Asymmetric Convolutions

### 3.2.2.2. Structure of Asymmetric Convolutions

If both the input and output filter counts are the same, the two-layer approach is 33% less expensive. This is how the inception module appears following the use of the first two optimization approaches.

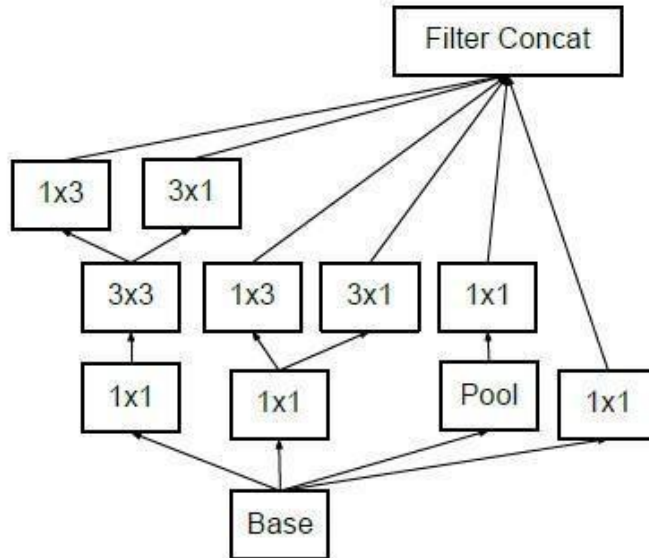


Figure 3.5: Structure of Asymmetric Convolutions

### 3.2.3. Utility of Auxiliary classifier

Auxiliary classifiers are used to accelerate the convergence of extremely deep neural networks. In very deep networks, the vanishing gradient problem is mostly addressed by the auxiliary classifier. Early on in the training, there was no improvement as a result of the auxiliary classifiers. However, as the experiment progressed, the network with auxiliary classifiers outperformed the network without auxiliary classifiers in terms of accuracy. As a result, the Inception V3 model architecture's auxiliary classifiers function as a regularize.

### 3.2.4. Efficient Grid Size Reduction

Traditionally, the grid size of the feature maps was decreased using average and maximum pooling. The activation dimension of the network filters is enhanced in the Inception V3 model to more effectively minimize the grid size.

For instance, reduction produces a  $d/2 \times d/2$  grid with  $2k$  filters from a  $d \times d$  grid with  $k$  filters. And two concurrent blocks of convolution and pooling that were subsequently concatenated are used to accomplish this.

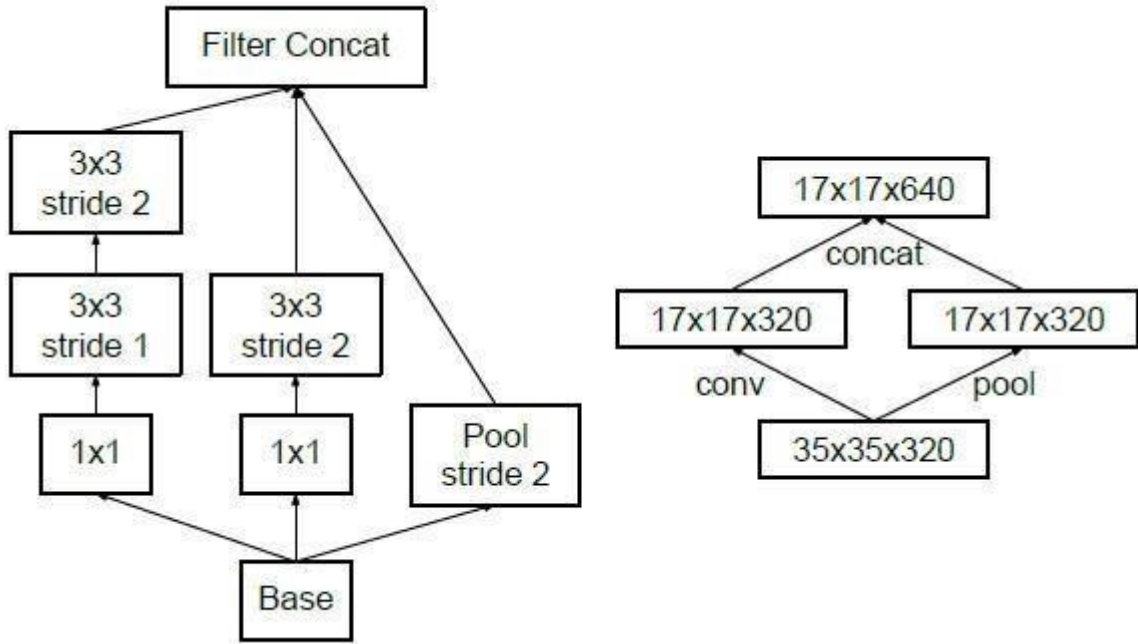


Figure 3.6: Efficient Grid Size Reduction

The aforementioned figure demonstrates how the grid size is effectively decreased while the filter banks are expanded.

### 3.2.5. Inception V3 Explanation

The final Inception V3 model after all the improvements seems like this:

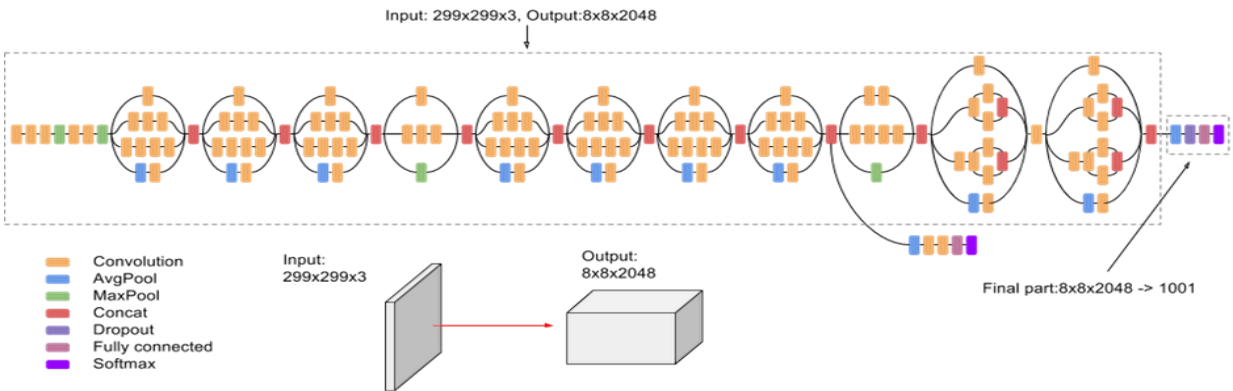


Figure 3.7: Inception V3 Architecture

The inception V3 model has 42 layers in total, which is a little more than the inception V1 and V2 models. However, this model's effectiveness is absolutely remarkable. We'll get to it shortly, but let's first take a closer look at the parts that make up the Inception V3 model.

TYPE	PATCH / STRIDE SIZE	INPUT SIZE
Conv	3×3/2	299×299×3
Conv	3×3/1	149×149×32
Conv padded	3×3/1	147×147×32
Pool	3×3/2	147×147×64
Conv	3×3/1	73×73×64
Conv	3×3/2	71×71×80
Conv	3×3/1	35×35×192
3 × Inception	Module 1	35×35×288
5 × Inception	Module 2	17×17×768
2 × Inception	Module 3	8×8×1280
Pool	8 × 8	8 × 8 × 2048
Linear	Logits	1 × 1 × 2048
Softmax	Classifier	1 × 1 × 1000

Figure 3.8: Inception V3 Model Layers

The inception V3 model's general structure is shown in the accompanying table. Each module's output size serves as the subsequent module's input size in this situation.

### 3.3. VGG16 Model

VGG16 is a VGG model variation with 16 convolution layers, and we have thoroughly investigated the VGG16 architecture.

VGGNet-16 has 16 convolutional layers and is desirable because to its relatively consistent architecture. It, like AlexNet, contains just 3x3 convolutions but a large number of filters. It may be trained on four GPUs for two to three weeks. It is now the most popular option for extracting features from photographs in the community. The VGGNet weight setting is freely accessible and has been utilized as a baseline feature extractor in many different applications and challenges.

It can be a little difficult to manage VGGNet's 138 million parameters, though. Transfer Learning can help people reach VGG. When the parameters are updated for greater precision and the model is pre-trained on a dataset, the parameter values may be used.

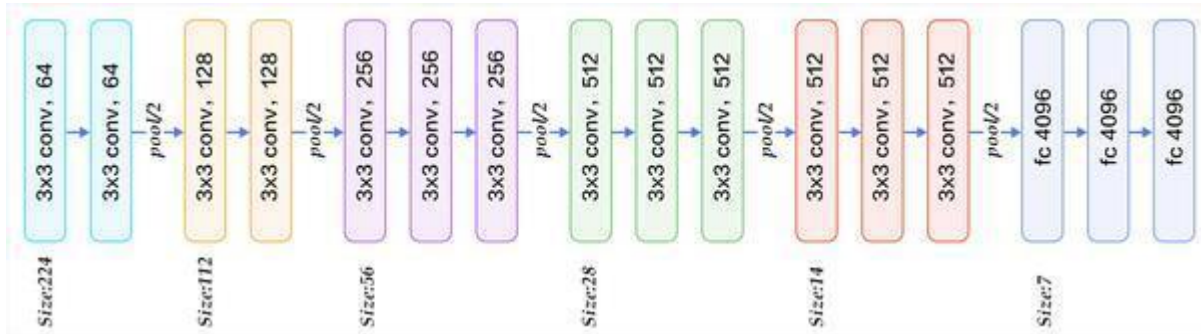


Figure 3.9: VGG16 Model Layers

### 3.3.1. 16 Layers of VGG16

The 16 layers that make up the VGG16 architecture are arranged into several categories. First, an input layer optimized for RGB pictures with 224x224 pixels is used. This is followed by two convolutional layers that work in tandem, each using 64 filters with 3x3 kernels and ReLU activation functions. Basic characteristics are extracted from the input by these first layers. Maxpooling layers with 2x2 windows decrease spatial dimensions after every pair of convolutional layers. The next layers build on this by adding more filters to 128, 256, and 512 in a similar manner, resulting in a hierarchy of features. Using softmax activation to output class probabilities, the final layer is a dense layer with as many neurons as there are classes in the classification problem. VGG16 is a popular and adaptable model for computer vision problems because of its 16 layers, which include both convolutional and fully linked layers. Table 3.1 depicting VGG 16 below:

Table 3.1 Layer of VGG16

Sr. No	Layer	No. of Filters
1	Convolution	64
2	Convolution + Max Pooling	64
3	Convolution	128
4	Convolution + Max Pooling	128
5	Convolution	256
6	Convolution	256
7	Convolution + Max Pooling	256
8	Convolution	512
9	Convolution	512
10	Convolution + Max Pooling	512
11	Convolution	512
12	Convolution	512
13	Convolution + Max Pooling	512
14	Fully Connected	4096
15	Fully Connected	4096
16	Output Layer with Softmax Activation	1000

### 3.3.2. VGG 16 Architecture

Convolutional neural networks (CNNs) with the VGG16 architecture are made for image categorization applications. It was created by the University of Oxford's Visual Geometry Group and is renowned for being straightforward and having good performance. The VGG16 architecture is described in further detail below:

**Input Layer:** Supports RGB images up to a preset resolution of 224 by 224 pixels.

**Convolutional Blocks (13 Convolutional Layers):** The five convolutional blocks that make up VGG16's deep stack of convolutional layers are what define it. Usually, a max-pooling layer comes



after two or more 3x3 convolutional layers in each block. As you move deeper into the network, the convolutional layers have more filters.

One pixel-wide 3x3 filters are used in convolutional layers. Max-pooling layers down sample the spatial dimensions using 2x2 windows with a stride of 2 pixels.

### Completely Networked Layers:

VGG16 features three fully connected (dense) layers that come after the convolutional layers.

With the exception of ImageNet's 1,000 classes, the first two fully linked layers each have 4,096 neurons, while the third layer has 1,000 neurons.

**Activation Function:** In the convolutional and fully connected layers, Rectified Linear Units (ReLU) are employed as activation functions.

**Softmax Layer:** To generate class probabilities for the input image, a softmax activation layer is placed after the last fully connected layer.

In conclusion, VGG16 is a good option for image classification tasks due to its deep architecture, which consists of 13 convolutional layers. It aided in the creation of deep learning for computer vision and functioned as a standard model for numerous image analysis problems.

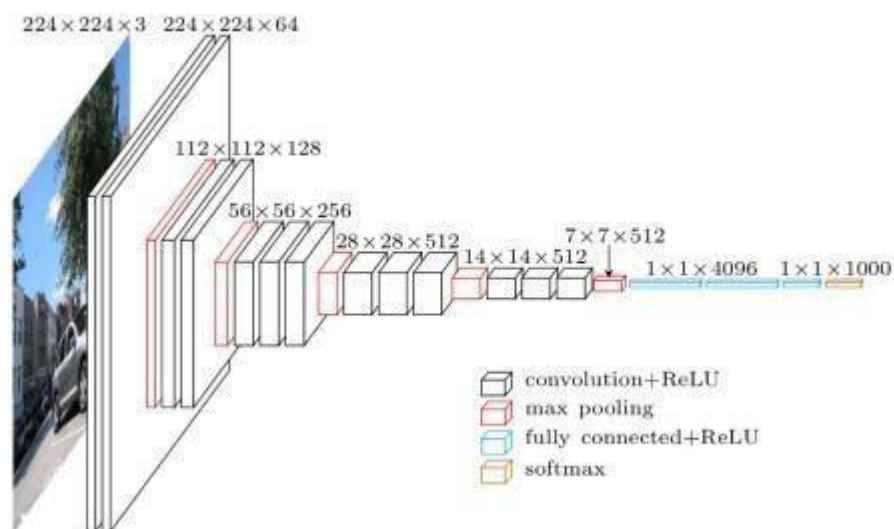


Figure 3.10: VGG 16 Architecture

## **3.4. VGG19 Model**

VGG19 is a variation of the VGG model that, in essence, has 19 levels (16 convolution layers, 3 Fully connected layer, 5 MaxPool layers and 1 SoftMax layer). Other VGG variations include VGG11, VGG16, and more. FLOPs in VGG19 total 19.6 billion.

AlexNet, which was released in 2012 and improved on conventional Convolutional neural networks, can be seen as the successor to AlexNet. However, VGG was developed by a different team at Oxford University, hence the name Visual Geometry Group. It takes some concepts from its predecessors and builds on them while using deep Convolutional neural layers to increase accuracy.

Let's examine VGG19, compare it to previous iterations of the VGG architecture, and examine some of the VGG architecture's beneficial and real-world applications.

Before getting started, let's look into what the VGG19 Architecture is and have a look at ImageNet and CNN in general.

### **3.4.1. Convolutional Neural Network(CNN)**

Let's first examine what ImageNet is. It is an image database with 14,197,122 pictures that are arranged in accordance with the WordNet hierarchical structure. This program aims to support image and vision researchers, students, and other stakeholders.

The ImageNet Large-Scale Visual Recognition Challenge (ILSVRC), one of the competitions it hosts, tasked researchers from around the world with developing solutions that would produce the lowest top-1 and top-5 error rates (the top-5 error rate would be the percentage of images where the correct label is not one of the model's five most likely labels). A validation set of 50,000 photos, a test set of 150 000 images, and a 1,000 class training set of 1.2 million images are provided for the competition.

### **3.4.2. VGG 19 Layers and Architecture**

Here's the VGG Architecture, which in 2014 outperformed other cutting-edge models and is still favored for many difficult tasks today.

VGG is a deep CNN that is used to identify pictures, to put it simply. The VGG19 model's layers Table 3.2 is as follows:

*Table 3.2 VGG 19 Layers*

Sr. No.	Layer	Shape	Filters
1	Convolution	3x3	64
2	Convolution	3x3	64
3	Max Pooling	-	-
4	Convolution	3x3	128
5	Convolution	3x3	128
6	Max Pooling	-	-
7	Convolution	3x3	256
8	Convolution	3x3	256
9	Convolution	3x3	256
10	Max Pooling	-	-
11	Convolution	3x3	256
12	Convolution	3x3	512
13	Convolution	3x3	512
14	Convolution	3x3	512
15	Convolution	3x3	512
16	Max Pooling	-	-
17	Convolution	3x3	512
18	Convolution	3x3	512
19	Convolution	3x3	512
20	Convolution	3x3	512
21	Max Pooling	-	-
22	Fully Connected (4096)	4096	-
23	Fully Connected (4096)	4096	-
24	Fully Connected (1000)	1000	-
25	Soft Max	-	-

### 3.4.3. VGG 19 Architecture

- This network received a fixed-size (224 \* 224) RGB picture as input, indicating that the matrix was shaped (224,224,3). The only preprocessing that was done is that they subtracted the mean RGB value from each pixel, computed over the whole training set.
- They covered the entire area of the image by using kernels of (3 \* 3) size with a stride size of 1 pixel.
- To maintain the image's spatial resolution, spatial padding was applied.
- Using stride 2, max pooling was carried out over a 2 \* 2 pixels' frame.
- Rectified linear unit (ReLU) was used after this to add non-linearity to the model in order to enhance classification accuracy and computation time. As opposed to earlier models that employed tanh or sigmoid functions, this one performed far better.
- Developed three fully linked layers, the first two of which had a size of 4096, followed by a layer with 1000 channels for classification using the 1000-way ILSVRC, and the third layer being a softmax function.

The VGG net was primarily created with the intention of winning the ILSVRC, but it has been used to many other uses as well.

- Used simply as a good classification architecture for several different datasets, and since the authors made the models accessible to the public, they may be used without modification for more jobs that are comparable.
- Transfer learning is also applicable to facial recognition tasks.
- With other frameworks, like as Keras, weights are conveniently accessible and may be adjusted and utilized anyway the user sees fit.
- Loss of style and content while utilizing VGG-19 network

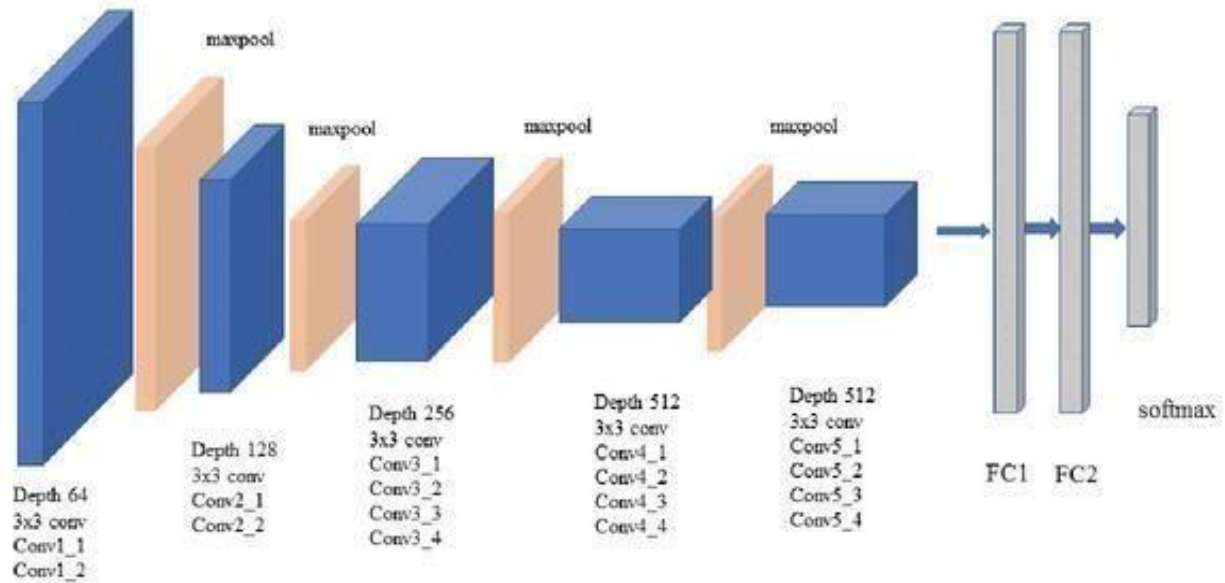


Figure 3.11: VGG 19 Architecture

### 3.5. Summary

The Inception V3 model, its main enhancements, and the introduction of the VGG16 and VGG19 models are covered in this chapter. Introduced in 2015, Inception V3 has 42 layers and is more accurate than its predecessors. Factorization into smaller convolutions, spatial factorization into asymmetric convolutions, the usefulness of auxiliary classifiers, and effective grid size reduction are the main enhancements in Inception V3. Each of these enhancements is thoroughly examined in this chapter.

1. The enhancements of Inception V3 may be summed up as follows:
2. For computational efficiency, factorization into smaller convolutions is used.
3. For increased model efficiency, include spatial factorization into asymmetric convolutions.
4. Auxiliary classifiers are used to solve vanishing gradient issues.
5. Effective decrease of grid size by improved activation dimension.

Overall, the chapter offers insights into these three well-known deep learning models, as well as their advances, architectural specifics, and uses in computer vision and image identification.

# Proposed Methodology & Framework

## 4.1. Overview of Proposed Methodologies

This chapter presents MixNet-LD, a novel system that uses dense blocks and convolutional neural networks (CNN) to categorize pictures of lung illnesses into several categories, such as pneumonia, lung cancer, COVID-19, normal, and tuberculosis (TB). Transfer learning is used to these dense blocks for training on lung-related problems, and the dense blocks are utilized to extract useful features. In this chapter, the systematic steps of the MixNet-LD system—seen in Figure 2—are explained. During training, features from dense blocks and CNN (MixNet) are integrated and continually enhanced.

A Support Vector Machine (SVM) classifier with a linear activation function is used to improve classification outcomes. For training and assessment, the authors use a dataset called PAKLUNGS, which consists of 13,313 images. PAK-LUNGS and other internet sources provide the dataset, and a trained pulmonologist has carefully chosen and classified each picture. For training and testing, three distinct datasets with various dimension settings are employed.

The process of adding new data points from preexisting ones in order to vary the dataset and enhance model performance while preventing over-fitting is known as data augmentation, and it is used in response to imbalances in data gathering. This chapter describes the Auto-Augment transformation policy and how to set up a transformation pipeline that includes the chosen AutoAugment policy, image resizing, and horizontal flipping.

A deep neural network called MixNet-LD model architecture is presented; it is intended to extract visual representations well while balancing computational economy and performance. To help with information flow between layers, it makes use of feature-mixing blocks with skip connections and mix-depth wise convolution blocks. Convolution layers, batch normalization, activation functions, and fully linked layers are also included in the model for feature processing and classification.

The chapter highlights that MixNet-LD's computational efficiency makes it appropriate for scenarios with limited resources, including mobile devices. It states that the model may be adjusted to perform certain functions, including recognizing HR in retinography images.

In summary, MixNet-LD is a potentially effective method for classifying lung illnesses from CT and X-ray pictures. It does this by using dense blocks in conjunction with CNN architecture to get precise findings.

## **4.2. Proposed Approach**

In this paper, a new system called MixNet-LD is developed, which mixes CNN (MixNet) with dense blocks. The MixNet-LD method is used to categorize lungs illness pictures into Normal, Pneumonia, Tuberculosis (TB), COVID-19, and Lung cancer. The dense blocks approach is used inside the MixNet-LD system to extract valuable attributes. Transfer learning of dense blocks is used to train on lungs-related defects. The MixNet-LD system includes critical mechanisms for detecting lung disease pictures and recognizing the problems described above. The systematic phases are visually depicted in Figure 2. The properties collected from CNN (MixNet) and the dense blocks are mixed, and the parameters of Dense Blocks are constantly improved throughout training. A feature transform layer is also developed to integrate characteristics via element-wise multiplication. Finally, to enhance classification results, an SVM classifier with a linear activation function is used.

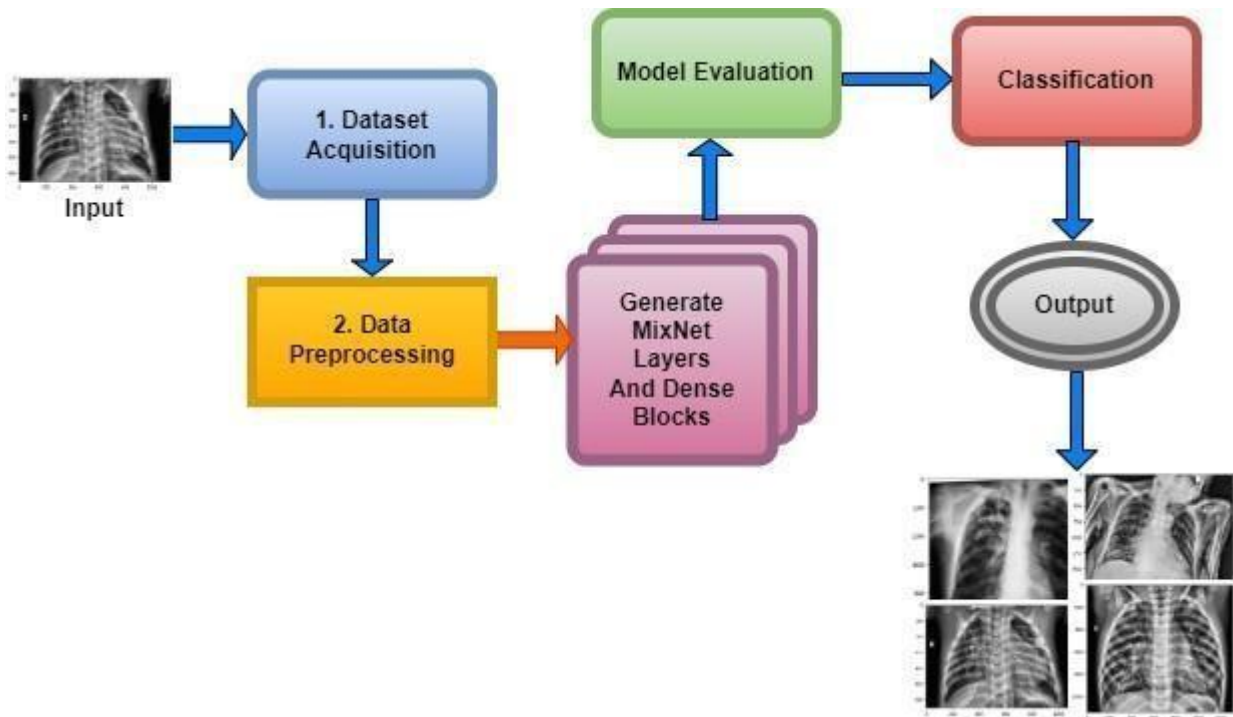


Figure 4.1: The MixNet-LD system's well-organized flow diagram for identifying lung illnesses

### 4.3. Dataset Acquisition and Pre-processing

A dataset named PAK-LUNGS, which contains 13,313 photos, was used to train and estimate the MixNet-LD model. Both PAK-LUNGS and well-known online sources were used as sources for the dataset. The Normal and Lungs diseases photos were manually isolated from the dataset acquired by a qualified pulmonologist to construct the training dataset. To detect lungs-related traits and establish a standard, the pulmonologist meticulously inspected 13,313 lungs photographs, as shown in Figure 1. The three datasets that were used to build the training and testing funds sets, each with a distinct dimension setting, are broken out in Table 4.1, 4.2. All photos used in the experiment were downsized to  $(700 \times 600)$  pixels, after which they were processed to create binary labels. 13,313 photos make up the whole dataset, of which 3,993 were used to test the system. To guarantee neutrality, the dataset was initially converted into a different classes dataset by balancing the total number of photos with and without the illness. Before being put into an algorithm created especially for the MixNet-LD model, the photos underwent preprocessing by being resized to  $(700 \times 600)$  pixels. To lessen the variation between data points, the photos were also standardized. Data from PAK-LUNGS is also used to train and assess the MixNet-LD system.



Each image was initially saved with a resolution of  $1125 \times 1264$  pixels. We applied Gran Cam technique for image pre-processing to clear the images features and remove the noise from the image shown in figure 4.1.

Using data from three separate sources, the photos were downsized to a more usual dimension of  $(700 \times 600)$  pixels in order to simplify and standardize the dataset. Furthermore, during the Dataset construction process, experienced pulmonologists contributed to the generation of both lungs' diseases and non-lungs diseases data for ground truth evaluation.

*Table 4.1 Image dataset of the lungs diseases for the MixNet-LD system*

Reference	Name	Normal	COVID-19	PNEUMONIA	TURBERCULOSIS	Total Images
[45]	Lungs Diseases Dataset	1,342	462	3,872	660	6,336
	(4 Types)					
Private	PAK-LUNGS	1,500	1500	1500	1500	6,000
		<b>2,842</b>	<b>1,962</b>	<b>5,372</b>	<b>2,160</b>	<b>12,336</b>

*Table 4.2. Image dataset of the lungs cancer for the MixNet-LD system*

Reference	Name	Normal	Cancer	Total Images
[46]	Chest CT-Scan images Dataset	154	473	627
Private	PAK-LUNGS	175	175	350
		<b>329</b>	<b>648</b>	<b>977</b>

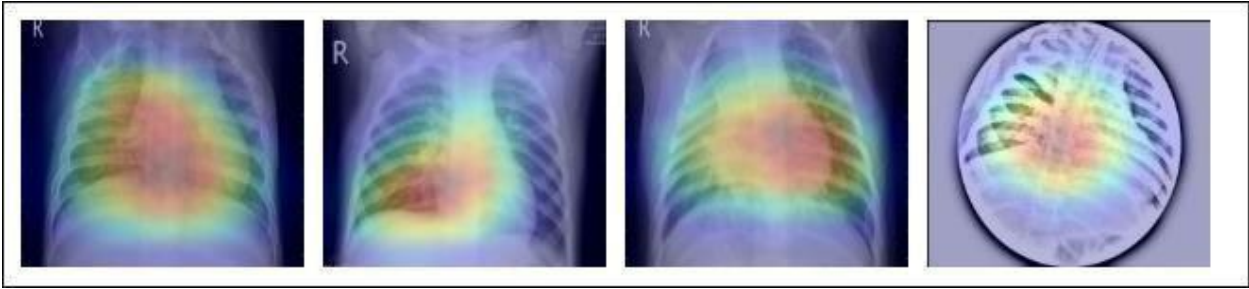


Figure 4.2: This image represents pre-processing results after Gran Cam technique.

#### 4.4. Data Augmentation

The dataset table makes it abundantly evident that the data collection was unequal, possibly resulting in bias towards a certain class during model training. This difficulty can be resolved via a technique known as "data augmentation" rather than by collecting additional data. By intentionally creating additional data points from the ones that already exist, data augmentation increases the dataset's diversity. This approach facilitates to expand and stabilize the model's execution while also guarding against overfitting. During training, pictures may be automatically enhanced using the AutoAugment approach, which enhances the generalisation of DL models. We describe the AutoAugment transformation policy, choosing either 'v1' or 'v2' for augmentation, and build a transformation pipeline that comprises picture resizing, applying horizontal flip, and the selected AutoAugment policy. The training pictures are then loaded from a custom dataset that is kept in a directory structure under the `./dataset/train` folder. The Data Loader is used to load the custom dataset, and the Image Folder class from `torchvision.datasets` aids in applying the Auto Augment transformation to each picture. In order to increase performance and generalization, a DL model may be trained on the custom dataset using batches of augmented photos that are provided by the Data Loader during training. Table 4.3, 4.4 represents the results of augmentation.

Table 4.3. Image dataset of the lungs diseases for the MixNet-LD system

<b>Normal</b>	<b>COVID-19</b>	<b>PNEUMONIA</b>	<b>TURBERCULOSIS</b>	<b>Total Images</b>
2000	1500	4000	1500	9,000
842	462	1,372	660	3,336
<b>2,842</b>	<b>1,962</b>	<b>5,372</b>	<b>2,160</b>	<b>12,336</b>

Table 4.4. Image dataset of the lungs cancer for the MixNet-LD system

<b>Normal</b>	<b>Cancer</b>	<b>Total Images</b>
500	500	1000
500	500	1000
<b>1000</b>	<b>1000</b>	<b>2000</b>

Table 4.5. Algorithm 1: Auto Augmentation

Steps	Explanation
1	Import the necessary libraries, including augmentations, torch vision, and torch.
2	Define the function <code>get_autoaugment_transform()</code> to create the Auto Augment transformation pipeline. The function uses augmentations to specify the
	Auto Augment policy and other image transformations. The resulting transformation pipeline will resize the images, apply horizontal flip, and normalize the pixel values.
3	<p>In the main part of the code:</p> <ul style="list-style-type: none"> <li>a. Load the custom dataset using Image Folder from torch vision. datasets.</li> <li>b. Apply the previously defined Auto Augment transformation to the dataset.</li> </ul>
4	Create a Data Loader using <code>torch.utils.data. Data Loader</code> . The Data Loader will handle batching and shuffling of the augmented dataset during training. Define a simple CNN model class Simple CNN using <code>cnn Module</code> .
5	Define a simple CNN model class Simple CNN using <code>CNN Module</code> . Set up the loss function (e.g., Cross Entropy Loss) and optimizer (e.g., SGD or Adam) for training the model. Specify the number of training epochs and other hyper parameters like learning rate and batch size.
6	<p>Train the model for the specified number of epochs:</p> <ul style="list-style-type: none"> <li>a. Set the model to training mode by calling <code>model.train()</code> .</li> <li>b. Loop through the Data Loader to obtain batches of augmented images and their corresponding labels.</li> <li>c. To get expected outputs, run the model via a forward pass.</li> <li>d. Calculate the difference between ground truth labels and expected outputs using the defined loss function.</li> <li>e. Perform a backward pass to compute gradients of the model's parameters with respect to the loss.</li> <li>f. Update the model's parameters using the chosen optimizer and the computed gradients.</li> <li>g. Optionally, you can validate the model's performance on a separate validation dataset during training.</li> </ul>
7	After training is complete, the model is ready for inference and evaluation on new data.

## 4.5. MixNet-LD Architecture

The MixNet-LD model is a deep neural network architecture created to effectively extract visual representations. MixNet-LD seeks a mix between performance and computational economy, drawing inspiration from the successful Inception and MobileNet models. Mix-depthwise convolutional blocks are used, which combine depth wise separable convolutions with different kernel sizes to enable effective feature extraction at various scales. Furthermore, feature-mixing blocks with skip connections allow information to move easily across layers, improving gradient propagation. Convolutional layers, batch normalization, and activation functions are used in the model to extract features and account for nonlinearity. For further feature processing, fully linked layers are employed after global average pooling to minimize spatial dimensions. To get class probabilities for classification problems, a softmax activation is used to the final output layer. Because of its emphasis on computational effectiveness, MixNet-LD is particularly suited for contexts with limited resources, such as mobile devices. The model gains superior performance in a variety of computer vision tasks, such as picture classification and object recognition, by being trained on a huge dataset of labelled images. MixNet-LD has to be fine-tuned on a fundus dataset that has been suitably labelled in order to be used for identifying HR in retinography pictures.

Below Fig 4.3 schematic diagram is shown.

The MixDepthwise Convolutional Block applies depthwise convolutions with different kernel sizes to the input feature map  $x$ . Then, for each convolution, it follows the sequence of Batch Normalization (BN), ReLU activation, and pointwise convolution with a  $1 \times 1$  kernel. Finally, the outputs obtained from all these convolutional paths are concatenated together.

$x$  be the input feature map to the MixDepthwise Convolutional Block.  $K$  be the set of kernel sizes used in the block.  $Conv_k(\cdot)$  represent the depthwise convolution operation with a kernel size  $k$ .  $Conv_{1 \times 1}(\cdot)$  represent the pointwise convolution operation with a  $1 \times 1$  kernel. The MixDepthwise Convolutional Block can be represented as follows:

$$MixDepthwiseBlock(x) = Concatenate([conv_{1 \times 1}(ReLU(BN(conv_k(x)))))]_{k \in K} \quad (1)$$

The Dense block is a standard building block in ResNet models, comprising two convolutions and a residual connection.  $x$  be the input feature map to the Dense block.  $F$  be the number of filters

(output channels) in the block.  $Conv(\cdot)$  represent the convolution operation. Shortcut be the identity shortcut (dense connection). The Dense Block can be represented as follows:

$$DenseBlock(x, F) = ReLU(BN(conv(x, F)) + shortcut) \quad (2)$$

The MixNet with Dense blocks can be represented as follows:

$$x = Conv2D(inputs, 64, (3,3), 'same') \quad (3)$$

$$x = ReLU(BN(x)) \quad (4)$$

$$x = MaxPooling2D(x, (2,2)) \quad (5)$$

$$x = MixDepthwiseBlock(x, K1) \quad (7)$$

$$x = MixDepthwiseBlock(x, K2) \quad (8)$$

$$x = DenseBlock(x, 128) \quad (9)$$

$$x = DenseBlock(x, 128) \quad (10)$$

$$x = Conv2D(x, 256, (3,3), 'same') \quad (11)$$

$$x = ReLU(BN(x)) \quad (12)$$

$$x = GlobalAveragePooling2D(x) \quad (13)$$

$$x = Dense(x, 256) = ReLU(BN(x)) \quad (14)$$

$$x = Dense(x, N, SVM) \quad (15)$$

Table 4.6. Algorithm 2: Working of the MixNet-DL model for feature map extraction

Steps	Explanation
1	<p>Define the MixDepthwise Convolutional Block:</p> <ul style="list-style-type: none"> <li>• Input: <math>x</math> (Input feature map), <math>K</math> (Set of kernel sizes used in the block) For each <math>k</math> in <math>K</math>:</li> <li>• Perform a depthwise convolution on <math>x</math> with kernel size <math>k</math>.</li> <li>• Apply Batch Normalization to the result. Apply ReLU activation to the result.</li> </ul> <p>Perform a pointwise convolution on the result with a <math>1 \times 1</math> kernel.</p> <ul style="list-style-type: none"> <li>• Concatenate the outputs of all the pointwise convolutions.</li> <li>• Output: Concatenated tensor representing the MixDepthwise Convolutional Block output.</li> </ul>
2	<p>Define the Dense block:</p> <ul style="list-style-type: none"> <li>• Input: <math>x</math> (Input feature map), <math>F</math> (Number of filters in the block)</li> <li>• Save <math>x</math> as the shortcut for the residual connection.</li> <li>• Perform a <math>3 \times 3</math> convolution on <math>x</math> with <math>F</math> filters and 'same' padding.</li> <li>• Apply Batch Normalization to the result.</li> <li>• Apply ReLU activation to the result.</li> <li>• Perform another <math>3 \times 3</math> convolution on the result with <math>F</math> filters and 'same' padding.</li> <li>• Apply Batch Normalization to the result. Add the result to the shortcut to create the residual connection. Apply ReLU activation to the result. Output: Output tensor representing the Dense block output.</li> </ul>

3	<p>Define the MixNet with ResNet model:</p> <ul style="list-style-type: none"> <li>• Input: inputs (Input tensor to the model) Perform a 3x3 convolution on inputs with 64 filters and 'same' padding.</li> <li>• Apply Batch Normalization to the result. Apply ReLU activation to the result.</li> <li>• Perform MaxPooling with a 2x2 pool size on the result.</li> <li>• Apply the MixDepthwise Convolutional Block on the result with 1 K 1 kernel sizes.</li> <li>• Apply the MixDepthwise Convolutional Block on the result with 2 K 2 kernel sizes.</li> <li>• Apply the Dense block on the result with 128 filters.</li> <li>• Apply the Dense block on the result with 128 filters. Perform a 3x3 convolution on the result with 256 filters and 'same' padding.</li> <li>• Apply Batch Normalization to the result. Apply ReLU activation to the result.</li> <li>• Perform Global Average Pooling on the result to reduce spatial dimensions.</li> <li>• Perform a Dense layer with 256 units on the result.</li> <li>• Apply Batch Normalization to the result.</li> </ul>
	<ul style="list-style-type: none"> <li>• Apply ReLU activation to the result. Perform a Dense layer with the number of classes (<math>N</math>) and SVM linear classifier activation for classification.</li> <li>• Output: Output tensor representing the final classification probabilities.</li> </ul>
4	<p>Example Usage:</p> <ul style="list-style-type: none"> <li>• Input shape: ( 224, 224, 3 ) # Adjust input shape based on your data</li> <li>• Number of classes: <math>N</math> (e.g., 10 for image classification with 10 classes)</li> </ul> <p>Instantiate the MixNet with ResNet model using the defined architecture and provided input shape and number of classes.</p> <ul style="list-style-type: none"> <li>• Compile the model using the proper metrics, loss function, and optimizer. for your specific classification task.</li> <li>• Train the model on your image dataset.</li> <li>• Estimate the simulation's performing on a separate test dataset.</li> </ul>



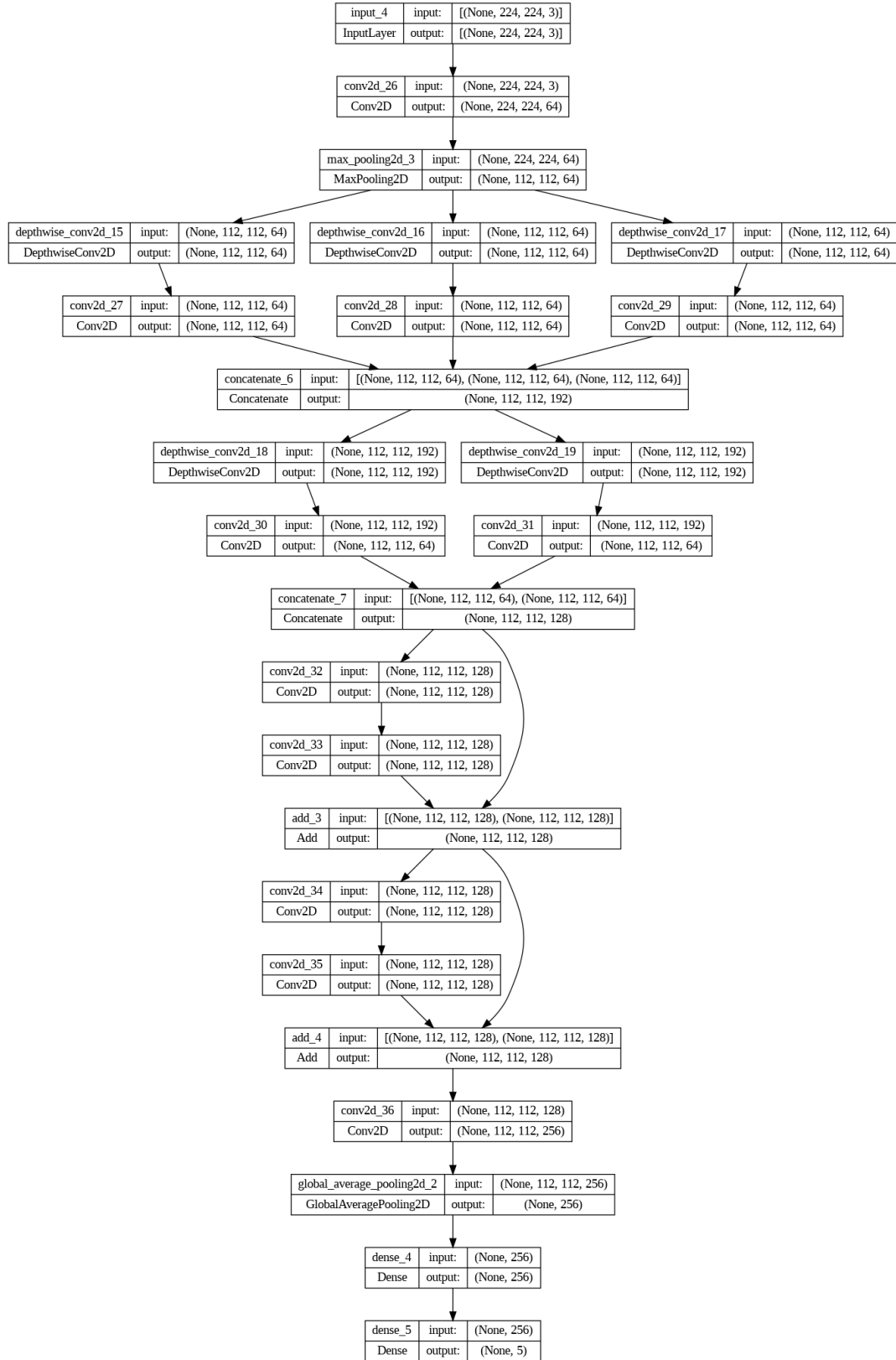


Figure 4.3: Schematic diagram of MixNet-LD

## 4.6. Recognition of Lungs Disease

Automatically recognizing lungs diseases from lungs X-ray and CT Scan images presents issues for CAD systems. The MixNet architecture is used to create the MixNet-LD method for effective picture classification in order to solve this. Figure 4 shows how skip links are put into the network to speed up learning. The name of the complete system is MixNet-LD. Multiple depth wise convolution layers are followed by ReLU activation, max pooling, and batch normalization layers to generate the dense layers in MixNet's dense blocks. To enable efficient training of the dense network, these layers are connected using skip connections. Three Dense Blocks (DBs) are used by MixNet-DL to efficiently construct trained three-CNN-feature maps with substantial depth, resulting in dense blocks. Each DB retains the same input and output sizes throughout the feature learning phase. The feature maps are produced by a factor of two down sampling from each DB. This model makes use of three DBs. To carry out the categorization process, the network's final fully linked output is enlarged with an extra layer. The dense learning sub-network's properties are successfully divided into two categories by this layer. The amount of nerve cell in this layer is maintained at 850 to guarantee peak performance. Batch normalisation layers are included in MixNet as a preprocessing step, which enhances the training of deep neural networks and model convergence. The following is a description of the batch normalisation formulae (Table 4.7):

$$B = \{X_{1\dots m}\}, \gamma, \beta \quad (16)$$

$$\{y_i = BN_{\gamma\beta}(X_i)\} \quad (17)$$

$$\mu_B \leftarrow \frac{1}{m} \sum_{i=1}^m X_i \quad (18)$$

$$\sigma_B \leftarrow \frac{1}{m} \sum_{i=1}^m X_i - \mu_B \quad (19)$$

$$X_i \leftarrow X_{\sigma^i B^2} + \mu \epsilon^B \quad (20)$$

$$y_i \leftarrow YX_i + \beta = BN_{\gamma\beta}(X_i) \quad (21)$$

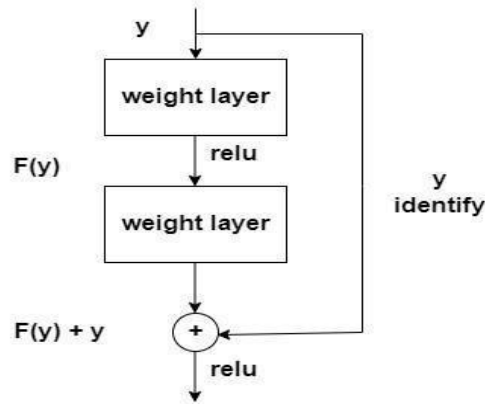


Figure 4.4: Dense Blocks

$$DB(z) = Output - Input = a(z) - z \quad (22)$$

$$a(z) = DB(z) + z \quad (23)$$

To improve its performance on job  $a(z)$ , the entire dense block functions by analysing the actual output. The layers are working hard to learn the residual,  $DB(z)$ , according to a close inspection of Fig. 4.4. because of the  $y$ -identity relationship. As a result, unlike traditional network layers that fully understand the output ( $a(z)$ ), the layers in a dense network learn about the dense  $DB(z)$ .

Table 4.7. Symbolization Table

Methods	Values
$\beta$ Batch	Batch
$x$ batch minimum activating value	batch minimum activating value
$\mu_B$ mini-batch mean	Mini-batch mean
$\sigma_{2B}$	Mini-batch variance
$\epsilon$	Adding a constant to ensure numerical stability
$\beta$	learning variable
$\gamma$	learning variable

## 4.7. LSVM

The linear SVM machine learning classifier, with a train-test splitting ratio of 75% to 25%, is used for the HR classification job. This decision was made because of how well linear SVM performs

overall and how well it handles tiny datasets. SVM is a classification approach that is well-known for being superior to other classifiers and is frequently used to solve practical issues. Instead of using conventional DL or machine learning classifiers, the authors chose to create a depth-wise separable CNN for computer vision or image classification problems. However, the Linear SVM classifier was chosen for the current study because it is excellent at handling tiny datasets although yet achieving well in high-dimensional environments. Given that the task required binary categorization, this choice made sense. In process to increase the effectiveness of their method and find the best hyperplane to distinguish between abnormal and healthy cells in retinal images, they also used linear SVM. Typically, an LSVM takes a vector  $Y = (z_1, z_2, \dots, z_n)$  and outputs a value  $y \in \mathbb{R}_n$  that may be written as:

$$Y_{out} = (Weig, Ziv) + c \quad (24)$$

Weig stands for the weight in Equation (24), while  $c$  is the offset. Weig and  $c$  are real-valued parameters that were both learnt during training and are a part of the real numbers ( $\mathbb{R}$ ) set. Dependent on whether  $y$  is larger than or less than 0, the input vector  $Ziv$  is classified as belonging to class 1 or class 2, as shown in Algorithm 3.

Table 4.8. Proposed LSVM classifier

Steps	Explanation
Input	Extracted feature map $x = (z1, z2, \dots, zn)$ with observations $x = 0,1$ , Test data $Z_{test}$
Output	Categorization of normal and abnormal sections
1	Primarily, the classifier and Kernel Regularize $L2$ parameters are labelled for optimization.
2	Creation of LSVM <b>a.</b> The $x = (z1, z2, \dots, zn)$ training procedure of LSVM is finished using obtained attributes by our Algorithm 2. <b>b.</b> For the production of the hyperplane, use Equation (21).
3	The class label is assigned for testing samples $z_{test}$ using the evaluation work of the equation further down. $Z_{test} = (Weig, Ziv) + c$

## 4.8. Summary

CNNs and dense blocks are used to classify lung diseases in MixNet-LD. The technique identifies photos as COVID-19, lung cancer, pneumonia, TB, and normal. Transfer learning trains for lung impairments, and dense blocks extract important features. MixNet-LD feature transform layers incorporate important lung disease algorithms and features. SVM classifiers with linear activation functions improve classification. Training and assessment use the 13,313-image PAK-LUNGS dataset from many sources. A skilled pulmonologist chooses data to determine lung features. Photos are standardised and reduced for data processing. MixNet-LD optimises feature extraction using skip connections, depth-wise convolutional blocks, and fully connected layers. Classification workloads and resource-constrained contexts like mobile devices benefit from this strategy.

Chapter covers HR classification classifier Linear Support Vector Machine (LSVM). LSVM was selected for short datasets and binary classification, MixNet-LD's creation, data preparation and augmentation, and LSVM's lung disease classification from medical pictures.

# Results and Experiments

## 5.1. Overview

A collection of 13,313 lungs pictures, including both high-resolution Normal and Diseased images, was used to train the MixNet-DL model. These lungs photos were obtained from credible Pakistani hospitals (Pak-Lungs) and a number of reliable online sources. All 13,313 images were downsized to  $(700 \times 600)$  pixels for feature extraction and classification activities. Utilizing MixNet and leftover building blocks, the MixNet-DL system underwent training for 100 epochs. The best model was found in the 30th era and achieved an excellent f1-score of 0.97. The accuracy (ACC), specificity (SP), and sensitivity (SE) values for the proposed MixNet-DL system were determined by statistical analysis. Then, these measurements were contrasted with those from other systems. A computer with an HP-i7 CPU, 8 cores, 32 GB of RAM, and a 2 GB Gigabyte NIVIDA GPU was used to build and develop the Incept-HR system. Windows 11 Professional 64-bit is the operating system used by this machine.

This chapter provide scientific or research work that compares and evaluates the effectiveness of several deep learning models, including Inception V3, ResNet, Xception, MixNet LD, and VGG16 and VGG19. The chapter is broken up into many parts, each of which describes an experiment and its findings:

It seems that the main goal of each experiment is to compare the suggested MixNet-DL model's performance with other deep learning models and assess its performance on various datasets. The results show that in terms of accuracy and other assessment measures, the MixNet-DL model performs well and often surpasses other models. Confusion matrices and loss measures are also shown to provide a thorough evaluation of the model's effectiveness.

## 5.2. Experiment 1: Performance Comparison between MixNet LD, VGG16, VGG19, Inception V3, ResNet

In association to estimate the execution of the DL models VGG16, VGG19, InceptionV3, ResNet, Xception and MobileNet with the proposed MixNet-DL system, we ran an experiment in this study. Notably, the same number of epochs was used to train each of these DL models. Two identical Deep Neural Networks were trained after the top network was determined based on validation accuracy. Table 6 exhibit the comparison findings between the MixNet-DL system and the VGG16, VGG19, InceptionV3, ResNet, Xception and MobileNet models in terms of sensitivity, specificity, accuracy, and area under the curve (AUC). According to the results, the MixNet-LD system performs better than other DL models, proving its superior performance.

Figure 5.1 represent the comparison between different DL model and MixNet-LD

Table 5.1. Performance comparison between MixNet-LD, VGG16, VGG19, InceptionV3, ResNet, Xception and MobileNet .

<b>Models</b>	<b>Sensitivity</b>	<b>Specificity</b>	<b>Accuracy</b>
VGG16	72	76	78.6
VGG19	75	77	79.2
InceptionV3	80.1	81.5	82.4
ResNet50	82.5	84.9	86.7
Xception	79.2	80.4	83.8
MobileNet	83.6	84.7	87.5
<b>MixNet-LD</b>	<b>95.2</b>	<b>96.7</b>	<b>97.7</b>

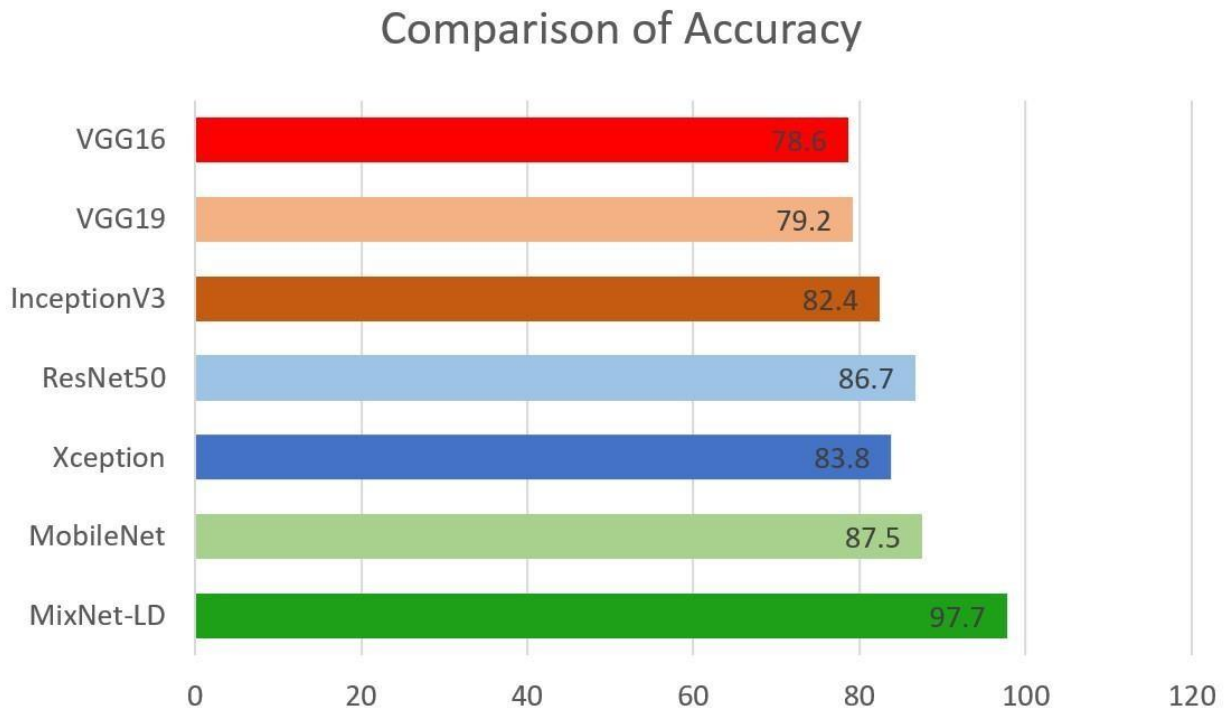


Figure 5.1: Comparison between different DL model and MixNet-LD

### 5.3. Experiment 2: Proposed Model Training and Validation Accuracy & Loss on Public Dataset

In this study, we use a dataset called "Lungs Diseases Dataset (4 Types)" which we downloaded from a reliable online source [45], to assess the performance of our suggested MixNet-DL approach. In the beginning, we used the appropriate datasets to compare the model's performance on the training and validation sets and to assess the loss function. The training and validation accuracy of the MixNet-DL model as it was trained on this dataset is shown visually in Figure 5.2,5.3. The outcomes unequivocally show how effectively our model works in both the training and validation settings. Furthermore, we obtained perfect accuracy on both the training and validation sets using the lungs dataset mentioned in Table 5.1.



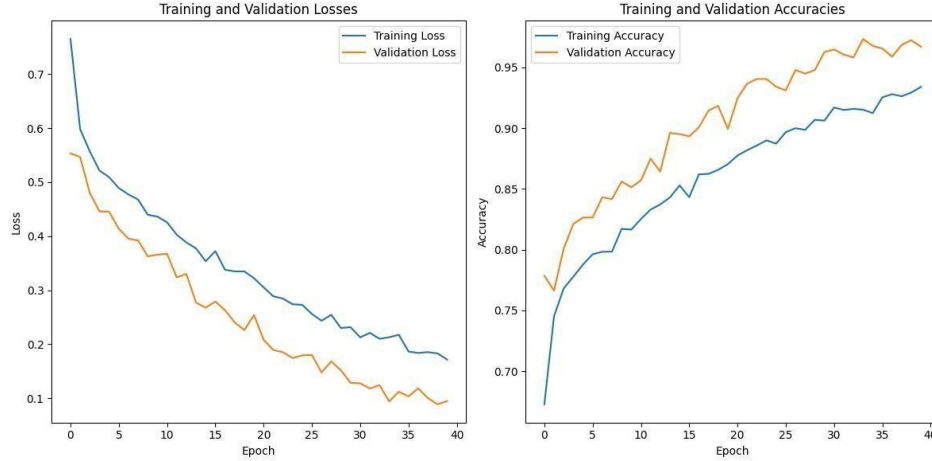


Figure 5.2: Represents the proposed model's training validation accuracy and loss.

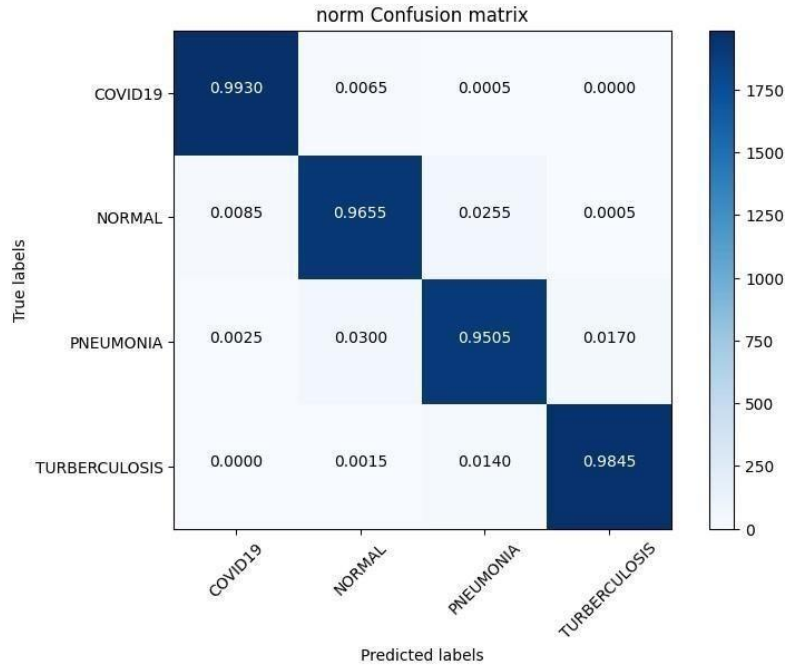


Figure 5.3: Confusion matrix of Lungs Diseases Dataset (4 Types)

### 5.4. Experiment 3: Proposed Model Training and Validation Accuracy & Loss on Public Dataset

In this investigation, we estimated the performance of our proposed MixNet-DL technique using PAK-LUNGS dataset. First, we evaluated the loss function and evaluated the representation's

operation on the training and validation sets using the Pak-Lungs dataset. The confusion matrix and training and validation accuracy of the MixNet-DL model when trained on this dataset is shown graphically in Figure 5.2, 5.3. The outcomes show our model's great efficacy in both training and validation settings. Additionally, we were able to obtain 99% accuracy on both the training and validation sets by using the Pak-Lungs dataset mentioned in Table 5.2.

Table 5.2. Performance assessment between Lungs Diseases Dataset (4 Types) and Pak-Lungs

Dataset	Sensitivity	Specificity	F1-Score	Recall	Accuracy
Lungs Diseases Dataset (4 Types) [45]	0.98	0.97	98	0.98	97.34
Pak-Lungs	0.99	0.98.5	0.988	0.99	0.99

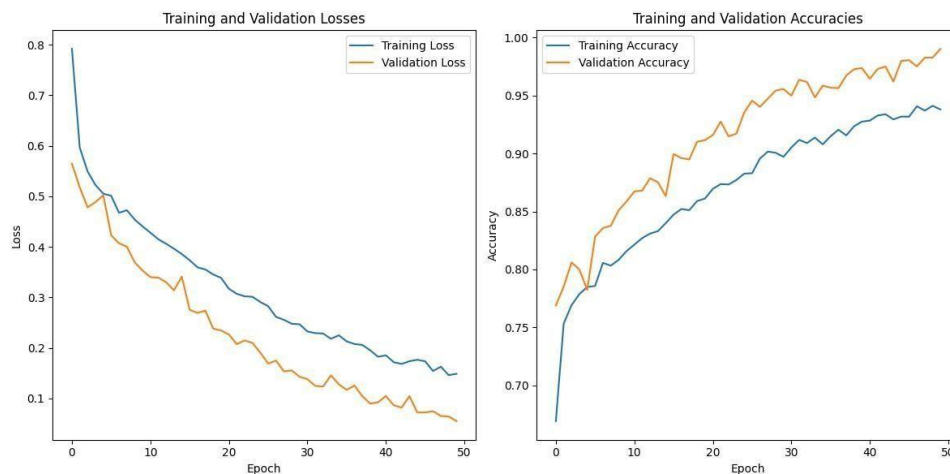


Figure 5.4: Represents the proposed model's training and validation accuracy and loss using Pak Lungs.

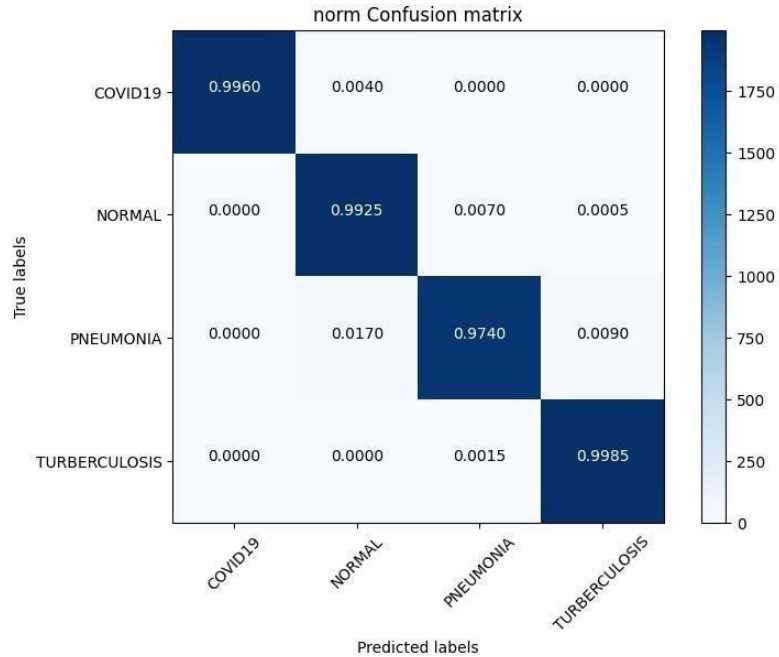


Figure 5.5: Confusion matrix of Pak-Lungs Dataset

### 5.5. Experiment 4: Performance Comparison between Chest CT-Scan Images Dataset & Pak Lungs (Cancer)

In this paper, we test the efficacy of our proposed MixNet-LD technique using a novel dataset named Pak-Lungs (Cancer) and Chest CT-Scan Images Dataset [46], which was collected from hospitals in Pakistan. We began by comparing performance of the model on both training and validation datasets, as well as assessing the loss function on the corresponding datasets. The accuracy of the MixNet-LD model during training and validation using this dataset is depicted in Figure 10,11. The findings show that our model performed exceptionally well in both the training and validation settings. Using the PAK-LUNGS dataset, we achieved good accuracy on both the training and validation sets. Additionally, we were able to obtain 98.2% accuracy on both the training and validation sets by using the Pak-Lungs (Cancer) and 99% accuracy on Chest CT-Scan Images Dataset [46] dataset. Both Comparisons are showing in Figure 5.6 & 5.7 and Table 5.3.

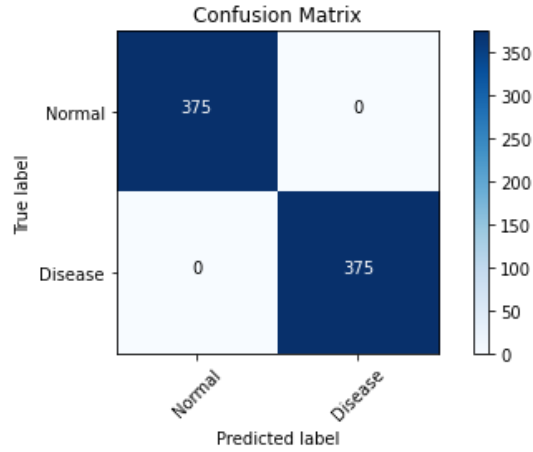


Figure 5.6: Confusion matrix of Pak-Lungs (Cancer)

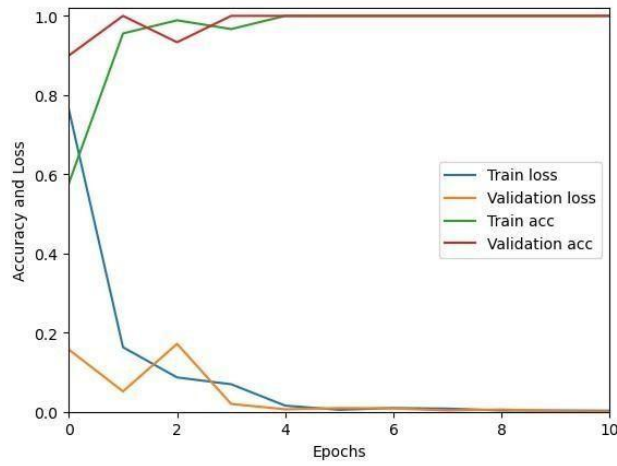


Figure 5.7: Training validation accuracy and loss on Pak-Lungs (Cancer)

Table 5.3. Performance comparison between Chest CT-Scan Images Dataset and Pak-Lungs (Cancer)

Dataset	Sensitivity	Specificity	F1-Score	Recall	Accuracy
Chest CTScan images Dataset [46]	0.98.2	0.99	99	0.99	99.34
Pak-Lungs (Cancer)	0.98.85	0.99	0.98.9	0.99	0.99.02

## 5.6. Summary

In the context of medical picture categorization, the chapter offers four experiments to assess the effectiveness of deep learning models, including MixNet LD, VGG16, VGG19, Inception V3, ResNet, Xception, and MobileNet. This is a succinct overview:

### **Experiment No. 1:**

- Evaluates and contrasts the results of several deep learning models.
- When compared to other models, MixNet-LD performs better in terms of sensitivity, specificity, accuracy, and AUC.

### **Experiment No. 2:**

- Uses the "Lungs Diseases Dataset (4 Types)" to evaluate the performance of the MixNetDL model.
- Obtains flawless precision on training and validation datasets.

### **Experiment No. 3:**

- Utilizes the PAK-LUNGS dataset to assess the MixNet-DL model.
- 99% accuracy is attained on training and validation datasets.

### **Experiment No. 4:**

- Uses the "Pak-Lungs (Cancer)" and "Chest CT-Scan Images Dataset" to test the MixNetLD model.
- Attains 98.2% and 99% accuracy, respectively, in training and validation sets, demonstrating good accuracy in both cases.

These results show that MixNet-LD is a promising option for medical picture classification tasks due to its remarkable performance in a variety of settings. Additionally, we were able to obtain 98.2% accuracy on both the training and validation sets by using the Pak-Lungs (Cancer) and 99% accuracy on Chest CT-Scan Images Dataset [46] dataset.

# Analysis and Discussion

## 6.1. Overview

This chapter offers a thorough summary of the state of the art at the moment for using deep learning to identify and categorize lung illnesses from X-ray pictures. It draws attention to the most recent developments in this area and compares two well-known models—VGG19+CNN and the groundbreaking MixNet-LD architecture.

The chapter begins by recognizing the limited previous research on identifying lung illnesses using X-ray pictures and deep learning algorithms, emphasizing the significance of recent advances. It presents the benchmark model, VGG19+CNN, emphasizing its diagnostic accuracy metrics, before introducing MixNet-LD as a breakthrough with improved performance. A carefully chosen dataset and pulmonologist validation are addressed, emphasizing the need of expert judgement and robust datasets. The revolutionary potential of MixNet-LD to revolutionize lung disease diagnostic precision is presented, spanning a variety of lung disorders. The chapter delves into the function of CNNs in lung disease diagnosis, as well as their importance during the COVID-19 epidemic. It goes beyond infectious illnesses to describe MixNet-LD's unique technique and the significance of the Pak-Lungs dataset. MixNet-LD practical applications in lung disease diagnosis are given, with an emphasis on its excellence and transformational potential in medical picture analysis. Finally, the chapter highlights MixNet-LD's position as a transformational instrument in healthcare and proposes future research objectives for its larger clinical use and efficacy development.

## 6.2. State of the Art Comparison

Only a few researchers have attempted to use deep learning methods to find lungs diseases in Xray pictures. The most recent research that uses DL for detecting lungs diseases in X-ray pictures is VGG19+CNN [14]. VGG19+CNN is state of the art deep learning model used for detecting lungs

diseases. It can be seen from Table 6.1 that MixNet-LD has a superior performance over VGG19 + CNN.

*Table 6.1. performance comparison between Incept-HR, Trivijoyo-2017 and CAD-HR*

<b>Methods</b>	<b>SE</b>	<b>Precision</b>	<b>ACC</b>	<b>AUC</b>
VGG19+CNN [14]	93.75%	97.56%	96.48%	0.96
<b>Proposed MixNet-LD</b>	<b>0.99</b>	<b>0.985</b>	<b>0.988</b>	<b>0.99</b>

Consequently, in comparison, the developed MixNet-LD system produced better results, with 99%, 99%, 99%, and 0.99 for SE, SP, ACC, and AUC, respectively. The identification accuracy in VGG19+CNN was 94.48%, according to the authors of this study [14]. Therefore, with the approval of expert pulmonologists, our MixNet-LD system was tested and trained on a balanced 13,313 images dataset. As a result, we achieved 99% accuracy in our classification, which is considered a big improvement over the state of the artwork. As a result, we achieved 99% accuracy in our classification which is considered a big improvement over the state of the artwork.

In the domain of leveraging deep learning methodologies for the detection of lung diseases from X-ray images, recent scholarly efforts have illuminated a captivating avenue of exploration. This investigation centred around a meticulous comparative analysis, shedding light on the nuanced distinctions between the well-established VGG19+CNN benchmark model and the innovative MixNet-LD architecture. The VGG19+CNN, a fusion of the VGG19 architecture's intricate feature extraction capabilities with a Convolution Neural Network (CNN) module, had previously garnered recognition for its performance metrics: sensitivity (SE) of 93.75%, precision of 97.56%, accuracy (ACC) of 96.48%, and an area under the curve (AUC) of 0.96. Counterbalancing this, the nascent MixNet-LD model exhibited an outstanding prowess, boasting sensitivity, precision, accuracy, and AUC values of 99%, 98.5%, 98.8%, and 0.99, respectively. The researchers, cognizant of the critical role of robust datasets, meticulously curated a balanced corpus of 13,313 X-ray images for comprehensive training and validation of MixNet-LD. Importantly, this novel model underwent rigorous evaluation under the supervision and endorsement of expert pulmonologists, consequently achieving a classification accuracy of 99%. This monumental leap forward in accuracy stands as a testament to MixNet-LD's transformative potential, poised to

elevate the accuracy and efficiency of lung disease diagnosis through X-ray imagery to unprecedented heights.

### **6.3. Discussion**

A number of lung diseases, including pneumonia, tuberculosis (TB), COVID-19, and lung cancer, may now be detected and classified thanks to substantial breakthroughs achieved by DLAs in the field of medical image analysis. With high rates of morbidity and mortality, these illnesses represent serious problems for public health internationally. For rapid treatment and better patient outcomes, it is essential to diagnose and classify these illnesses as early as possible. CNNs have demonstrated excellent performance in the diagnosis of lung illnesses in recent years. DL models for analyzing chest X-rays have been developed in part as a result of research which introduced the ChestX-ray8 dataset. The basis for identifying pneumonia and other thoracic illnesses has been established using this dataset in conjunction with weakly-supervised classification and localization approaches. For effective picture classification, introduced multi-scale dense networks utilizing deep CNN architectures. By extracting hierarchical characteristics, this method has proven effective in reliably detecting lung illnesses.

The COVID-19 pandemic's advent presented an important necessity for accurate and speedy detection. An artificial intelligence system can distinguish COVID-19 from community-acquired pneumonia in chest CT images. This method helps identify COVID-19 patients by utilizing DL techniques, which improves disease treatment and control. A DL model for automatic pulmonary TB categorization on chest radiography. Their approach enabled rapid screening and diagnosis by precisely identifying TB-related abnormalities. DL's application to COVID-19 diagnosis has drawn a lot of interest. Transfer learning and CNNs to identify COVID-19 in X-ray pictures. Their method showed how DL may help radiologists and other healthcare professionals swiftly identify COVID-19 patients. With a focus on interstitial lung illnesses, developed a deep CNN for lung pattern classification. In addition, developed and evaluated an AI system for COVID-19 diagnosis that correctly identified COVID-19 patients from imaging data by using DL techniques.

Along with infectious diseases, the diagnostic potential of DL models for lung cancer has also been thoroughly investigated. An image-based DL system is capable of identifying medical diagnoses,



such as lung cancer. This model illustrated how DL may be used to detect lung cancer and other diseases.

An important development in the field of medical image analysis is the planned MixNet-LD system for the automatic identification and classification of lung diseases. The lungs are essential for the respiratory system, and they must function properly for the body to exchange oxygen and carbon dioxide. However, a number of illnesses can impact on the lungs, having negative health effects. Since it might be difficult to identify and extract the lesion characteristics connected to lung problems, early and precise diagnosis of lung diseases is crucial for prompt and effective therapy. In order to solve this problem, the MixNet-LD system combines the strength of MixNet, a special pre-trained model, with dense blocks. By minimizing noise and emphasizing abnormalities, the suggested preprocessing technique utilizing CLAHE and MSR improves the quality of pictures of lung illness, further enhancing the classification performance. In order to correct the dataset's class imbalance and avoid over fitting, data augmentation techniques are also used, strengthening, and improving the MixNet-LD model.

The creation of the Pak-Lungs dataset, which consists of 6,000 photos of lung diseases gathered from reliable online sources and Pakistani hospitals, is a significant addition to the study. The MixNet-LD model was able to successfully handle a variety of lung illness cases thanks to this sizable dataset, achieving an amazing accuracy of 98.5% on the difficult lung disease dataset. Further demonstrating the superiority of the MixNet-LD system, which exceeds previous techniques with a substantially higher accuracy of 95%, is the comparison with state-of-the-art methods in medical image processing. As it offers a trustworthy and automated way for correctly diagnosing Normal, COVID-19, Pneumonia, Tuberculosis, and Lung Cancer illnesses, the system's performance has the potential to have real-world ramifications in medical diagnosis and therapy.

The MixNet-LD system is successful because it combines MixNet with dense blocks and makes use of data augmentation methods. While MixNet's pre-trained model offers the benefit of transfer learning, allowing the system to learn from past knowledge and attain cutting-edge performance, the dense blocks allow the extraction of critical characteristics from the pictures. The use of data augmentation approaches makes the model more flexible and able to handle a variety of lung illness situations while lowering the danger of over-fitting.

Overall, the MixNet-LD method better presented state-of-the-art methods and has excellent performance, making it an important tool in medical image analysis. It can also handle a variety of lung disease scenarios. The MixNet-LD system can dramatically boost patient outcomes and healthcare management by delivering accurate and timely diagnostics of lung illnesses. Further investigation can look at the possibilities of the MixNet-LD system in various clinical contexts as well as the applicability of the technology to other medical image analysis jobs. The system's breadth and influence in the field of medical imaging may be increased by ongoing improvement and optimization, which will ultimately lead to more efficient medical image processing in clinical settings.

## **6.4. Summary**

The performance of two deep learning models—VGG19+CNN and MixNet-LD—for the identification of lung conditions from X-ray pictures was compared by the researchers in this chapter. The MixNet-LD model surpassed the VGG19+CNN model with sensitivity, precision, accuracy, and AUC values of 99%, 98.5%, 98.8%, and 0.99, respectively. The VGG19+CNN model attained sensitivity of 93.75%, precision of 97.56%, accuracy of 96.48%, and an AUC of 0.96. After training on a balanced dataset of 13,313 pictures, the MixNet-LD model outperformed the state of the art with a classification accuracy of 99%.

Because lung disorders have an influence on public health, the chapter addresses the significance of early and correct detection of lung diseases, including pneumonia, TB, COVID-19, and lung cancer. It draws attention to how convolution neural networks (CNNs), in particular, play a key role in the diagnosis of various illnesses using chest X-ray pictures. The use of DL methods for COVID-19 and tuberculosis detection is also covered in this chapter.

A novel method for lung disease diagnosis is presented: The MixNet-LD system. It employs data augmentation methods and combines MixNet with dense blocks. It has the ability to accurately handle a wide range of lung disease situations, which makes it an important tool for medical picture analysis. Future research opportunities in various clinical settings and medical image analysis applications are offered, and the system's potential influence on patient outcomes and healthcare administration is stressed. In general, MixNet-LD performs better than other methods and shows promise for improving clinical image processing for medical purposes.

# Conclusion

## 7.1. Conclusion

In conclusion, the study presented a robust and innovative deep learning architecture for the accurate categorization of chest disorders using both Chest-X-Rays (CXR) and CT images. By combining a Convolution Neural Network (CNN) for feature extraction with the feature-rich MixNet-LD pre-trained model and a fully connected network for classification, the proposed methodology achieved remarkable results across multiple performance metrics.

The results of the experimental analysis showcased the superior performance of the MixNet-LD model in comparison to previous techniques. With an impressive sensitivity, specificity, F1Score, Recall, and accuracy all reaching 0.99, and an area under the curve (AUC) of 99%, the model exhibited a high degree of accuracy and reliability in diagnosing chest disorders, including Normal, COVID-19, Pneumonia, Tuberculosis, and Lung Cancer. This high level of accuracy holds significant promise for enhancing patient outcomes and improving healthcare management.

Moreover, the study provided valuable insights into the potential of CT scans for identifying abnormal patterns even before clinical symptoms manifest. This indicates the possibility of leveraging medical imaging as a powerful tool for early disease detection and intervention, which could profoundly impact disease prognosis and treatment success.

## 7.2. Future Work

Looking ahead, there are several exciting avenues for future research and development in this domain. The concept of fusing CXR and CT images holds promise for further enhancing diagnostic accuracy and comprehensiveness. The integration of different modalities can potentially provide a more holistic understanding of chest disorders, leading to even earlier and more accurate diagnoses.

Furthermore, exploring alternative deep learning architectures such as NASNet, MobileNet, and EfficientNet models could yield valuable insights into their performance and suitability for this

specific application. These models could potentially offer unique advantages in terms of efficiency, speed, and interpretability, which are critical factors in the medical field.

In addition, the continual expansion of datasets, encompassing diverse populations and a wide range of disease stages, could significantly contribute to refining and validating the proposed models. A larger and more diverse dataset would further strengthen the robustness and generalization capabilities of the deep learning architecture.

As the field of medical image analysis continues to advance, the fusion of cutting-edge AI techniques with clinical expertise is poised to revolutionize disease diagnosis and management. The study's success in developing a high-performance model for chest disorder classification marks an important step forward, offering tangible benefits for patient care. By building upon the foundations laid by this study, researchers can continue to drive innovation, uncover new insights, and ultimately improve healthcare outcomes for individuals affected by chest disorders.

#### **Data Availability Statement**

The datasets generated during and/or analyzed during the current study are available from the corresponding author on reasonable request.

## References

1. Wang, X., Peng, Y., Lu, L., Lu, Z., Bagheri, M., & Summers, R. M. (2017). ChestX-ray8: Hospital-scale chest X-ray database and benchmarks on weakly-supervised classification and localization of common thorax diseases. In Proceedings of the IEEE conference on computer vision and pattern recognition (pp. 2097-2106).
2. Shen, W., Zhou, M., Yang, F., Yang, C., Tian, J., & Wang, K. (2019). Multi-scale dense networks for resource-efficient image classification. *Pattern Recognition*, 85, 54-66.
3. Li, L., Qin, L., Xu, Z., Yin, Y., Wang, X., Kong, B., ... & Ai, L. (2020). Artificial intelligence distinguishes COVID-19 from community acquired pneumonia on chest CT. *Radiology*, 296(2), E65-E71.
4. Lakhani, P., & Sundaram, B. (2017). DL at chest radiography: Automated classification of pulmonary tuberculosis by using convolutional neural networks. *Radiology*, 284(2), 574582.
5. Apostolopoulos, I. D., & Mpesiana, T. A. (2020). Covid-19: automatic detection from xray images utilizing transfer learning with convolutional neural networks. *Physical and Engineering Sciences in Medicine*, 43(2), 635-640.
6. Anthimopoulos, M., Christodoulidis, S., Ebner, L., Christe, A., Mougiakakou, S., & Ebner, L. (2016). Lung pattern classification for interstitial lung diseases using a deep convolutional neural network. *IEEE transactions on medical imaging*, 35(5), 1207-1216.
7. Jin, C., Chen, W., Cao, Y., Xu, Z., Tan, Z., Zhang, H., ... & Zhang, J. (2020). Development and evaluation of an AI system for COVID-19 diagnosis. medRxiv.
8. Rajpurkar, P., Irvin, J., Ball, R. L., Zhu, K., Yang, B., Mehta, H., ... & Ng, A. Y. (2017). DL for chest radiograph diagnosis: A retrospective comparison of the CheXNeXt algorithm to practicing radiologists. *PLoS medicine*, 15(11), e1002686.
9. Lopes, A. J., Capone, D., Mogami, R., Godoy, I., Gazzotti, M. R., Roscani, M. G., ... & Jansen, J. M. (2020). Assessment of a DL system for tuberculosis screening on chest radiographs in high-risk populations. *JAMA network open*, 3(10), e2023249.

10. Kermany, D. S., Goldbaum, M., Cai, W., Valentim, C. C., Liang, H., Baxter, S. L., ... & Zhang, K. (2018). Identifying medical diagnoses and treatable diseases by image-based DL. *Cell*, 172(5), 1122-1131.
11. Wang, G., et al. (2021). DL for lung cancer classification: A comprehensive review. *IEEE Reviews in Biomedical Engineering*, 14, 134-149.
12. Rajpurkar, P., et al. (2017). CheXNet: Radiologist-level pneumonia detection on chest Xrays with DL. arXiv preprint arXiv:1711.05225.
13. V. Perumal, V. Narayanan, S.J.S. Rajasekar, Detection of COVID-19 using CXR and CT images using Transfer Learning and Haralick features, *Appl. Intell.* 51 (1) (2021) 341– 358, <https://doi.org/10.1007/S10489-020-01831-Z/FIGURES/11>.
14. R.K. Singh, R. Pandey, R.N. Babu, COVIDScreen: explainable DL framework for differential diagnosis of COVID-19 using chest X-rays, *Neural Comput. Appl.* 33 (14) (2021) 8871– 8892, <https://doi.org/10.1007/s00521-020-05636-6>.
15. S.K. Lakshmanaprabu, S.N. Mohanty, K. Shankar, N. Arunkumar, G. Ramirez, Optimal DL model for classification of lung cancer on CT images, *Futur. Gener. Comput. Syst.* v92 (2019) 374–382, <https://doi.org/10.1016/j.future.2018.10.009>.
16. Q.Z. Song, L. Zhao, X.K. Luo, X.C. Dou, Using DL for Classification of Lung Nodules on Computed Tomography Images, *J. Healthc. Eng.* (2017), <https://doi.org/10.1155/2017/8314740>.
17. G.A.P. Singh, P.K. Gupta, Performance analysis of various machine learningbased approaches for detection and classification of lung cancer in humans, *Neural Comput. Appl.* 31 (10) (2019) 6863–6877, <https://doi.org/10.1007/s00521-018-3518-x>
18. N. Kalaivani, N. Manimaran, S. Sophia, D.D. Devi, DL Based Lung Cancer Detection and Classification, *IOP Conf. Ser. Mater. Sci. Eng.* 994 (1) (2020) 7731–7776, <https://doi.org/10.1088/1757-899X/994/1/012026>.
19. A. Narin, C. Kaya, Z. Pamuk, Automatic detection of coronavirus disease (COVID-19) using X-ray images and deep convolutional neural networks, *Pattern Anal. Appl.* 24 (3) (2021) 1207–1220, <https://doi.org/10.1007/s10044-021-00984-y>.
20. G. Jia, H.K. Lam, Y. Xu, Classification of COVID-19 chest X- Ray and CT images using a type of dynamic CNN modification method, *Comput. Biol. Med.* 134 (2020), <https://doi.org/10.1016/j.combiomed.2021.104425>

21. S.H. Kassania, P.H. Kassanib, M.J. Wesolowskic, K.A. Schneidera, R. Detersa, Automatic Detection of Coronavirus Disease (COVID-19) in X-ray and CT Images: A Machine Learning Based Approach, *Biocybern. Biomed. Eng.* 41 (3) (2021) 867–879, <https://doi.org/10.1016/j.bbe.2021.05.013>
22. C. Li, D. Dong, L. Li, W. Gong, X. Li, Y. Bai, M. Wang, Z. Hu, T. Zha, J. Tian, Classification of Severe and Critical Covid-19 Using DL and Radiomics, *IEEE J. Biomed. Heal. Informatics* 24 (12) (2020) 3585–3594, <https://doi.org/10.1109/JBHI.2020.3036722>.
23. J. Shi, X. Yuan, M. Elhoseny, X. Yuan, Weakly Supervised DL for Objects Detection from Images 8 (2020) 231– 242, doi: 10.1007/978-3-030-45099-1\_18.
24. D. Dansanan, R. Kumar, A. Bhattacharjee, D.J. Hemanth, D. Gupta, A. Khanna, O. Castillo, Early diagnosis of COVID-19- affected patients based on X-ray and computed tomography images using DL algorithm, *Soft Comput.* (0123456789) (2020), <https://doi.org/10.1007/s00500-020-05275-y>.
25. D. Ezzat, A.E. Hassanien, H.A. Ella, An optimized DL architecture for the diagnosis of COVID-19 disease based on gravitational search optimization, *Appl. Soft Comput.* 98 (2021), <https://doi.org/10.1016/j.asoc.2020.106742> 106742.
26. V. Ravi, H. Narasimhan, C. Chakraborty, T.D. Pham, DL-based meta-classifier approach for COVID-19 classification using CT scan and chest X-ray images, *Multimed. Syst.* (0123456789) (2021), <https://doi.org/10.1007/s00530-02100826-1>.
27. Y. Pathak, P.K. Shukla, A. Tiwari, S. Stalin, S. Singh, Deep Transfer Learning Based Classification Model for COVID-19 Disease, *Irbm* 1 (2020) 1–6, <https://doi.org/10.1016/j.irbm.2020.05.003>.
28. A. Gupta, Anjum, S. Gupta, R. Katarya, InstaCovNet-19: A DL classification model for the detection of COVID- 19 patients using Chest X-ray, *Appl. Soft Comput.* 99 (2021) 106859, <https://doi.org/10.1016/j.asoc.2020.106859>.
29. K.F. Monowar, M.A.M. Hasan, J. Shin, Lung Opacity Classification With Convolutional Neural Networks Using Chest X-rays, 2020 11th International Conference on Electrical and Computer Engineering (ICECE), (2020), 169-172, doi: 10.1109/ICECE51571.2020.9393135.

30. J.E. Luján-García, M.A. Moreno-Ibarra, Y. Villuendas-Rey, C. Yáñez-Márquez, Fast COVID-19 and pneumonia classification using chest X-ray images, *Mathematics* 8 (2020) 9, <https://doi.org/10.3390/MATH8091423>.
31. S. Goyal, R. Singh, Detection and classification of lung diseases for pneumonia and Covid19 using machine and DL techniques, *J. Ambient Intell. Humaniz. Comput.* (0123456789) (2021), <https://doi.org/10.1007/s12652-021-03464-7>.
32. K. El Asnaoui, Design ensemble DL model for pneumonia disease classification, *Int. J. Multimed. Inf. Retr.* 10 (1) (2021) 55–68, <https://doi.org/10.1007/s13735021-00204-7>.
33. I. Sirazitdinov, M. Kholiavchenko, T. Mustafaev, Y. Yixuan, R. Kuleev, B. Ibragimov, Deep neural network ensemble for pneumonia localization from a largescale chest x-ray database, *Comput. Electr. Eng.* 78 (2019) 388–399, <https://doi.org/10.1016/j.compeleceng.2019.08.004>.
34. M.R. Lascu, DL in Classification of Covid-19 Coronavirus, Pneumonia and Healthy Lungs on CXR and CT Images, *J. Med. Biol. Eng.* 41 (4) (2021) 514–522, <https://doi.org/10.1007/s40846-021-00630-2>.
35. O. Stephen, M. Sain, U.J. Maduh, D.U. Jeong, An Efficient DL Approach to Pneumonia Classification in Healthcare, *J. Healthc. Eng.* (2019), <https://doi.org/10.1155/2019/4180949>.
36. J.E. Luján-García, C. Yáñez-Márquez, Y. Villuendas-Rey, O. Camacho-Nieto, A transfer learning method for pneumonia classification and visualization, *Appl. Sci.* 10 (8) (2020), <https://doi.org/10.3390/APP10082908>.
37. M. Rahimzadeh, A. Attar, A modified deep convolutional neural network for detecting COVID-19 and pneumonia from chest X-ray images based on the concatenation of Xception and ResNet50V2, *Inform. Med. Unlocked* 19 (2020), <https://doi.org/10.1016/j.imu.2020.100360>.
38. C. Sitaula, M.B. Hossain, Attention-based VGG-16 model for COVID-19 chest X-ray image classification, *Appl. Intell.* 51 (5) (2021) 2850–2863, <https://doi.org/10.1007/s10489-020-02055-x>



39. S. Sathitratanacheewin, P. Sunanta, K. Pongpirul, Deep learning for automated classification of tuberculosis-related chest X-Ray: dataset distribution shift limits diagnostic performance generalizability, *Heliyon* 6 (8) (2020) e04614.
40. X.W. Gao, C. James-Reynolds, E. Currie, Analysis of tuberculosis severity levels from CT pulmonary images based on enhanced residual DL architecture, *Neurocomputing* 392 (2020) 233–244, <https://doi.org/10.1016/j.neucom.2018.12.086>
41. R. Hooda, A. Mittal, S. Sofat, Automated TB classification using ensemble of deep architectures”, *Multimed. Tools Appl.* 78 (22) (2019) 31515–31532, <https://doi.org/10.1007/s11042-019-07984-5>.
42. T.B. Chandra, K. Verma, B.K. Singh, D. Jain, S.S. Netam, Automatic detection of tuberculosis related abnormalities in Chest X-ray images using hierarchical feature extraction scheme, *Expert Syst. Appl.* 158 (2020), <https://doi.org/10.1016/j.eswa.2020.113514> 113514.
43. Shahin, Osama R., Hamoud H. Alshammari, Ahmed I. Taloba, Rasha M. Abd El-Aziz, Machine Learning Approach for Autonomous Detection and Classification of COVID-19 Virus, *Comput. Electr. Eng.* 101 (2022) 108055.
44. Shahin, Osama R., Rasha M. Abd El-Aziz, Ahmed I. Taloba, Detection and classification of Covid-19 in CT-lungs screening using machine learning techniques, *J. Interdisciplinary Math.* 25 (3) (2022) 791-813.
45. Lungs Disease Dataset (4 types). (n.d.). [Www.kaggle.com](http://www.kaggle.com). Retrieved July 28, 2023, from <https://www.kaggle.com/datasets/omkarmanohardalvi/lungs-disease-dataset-4-types>
46. “Chest CT-Scan Images Dataset.” [Www.kaggle.com](http://www.kaggle.com), [www.kaggle.com/datasets/mohamedhanyyy/chest-ctscan-images](http://www.kaggle.com/datasets/mohamedhanyyy/chest-ctscan-images).